SCK•CEN

STUDIECENTRUM VOOR KERNENERGIE
CENTRE D'ÉTUDE DE L'ÉNERGIE NUCLÉAIRE

PRESSURE VESSEL STEEL RESEARCH: BELGIAN ACTIVITIES

E. van Walle, A. Fabry, H. Aït Abderrahim, R. Chaouadi, P. D'hondt, J.L. Puzzolante, J. Van de Velde and T. Van Ransbeeck

SCK•CEN, Mol, Belgium

R. Gerard

Tractebel, Brussels, Belgium

IAEA Specialists Meeting on Advanced Structural Integrity Assessment Procedures

Argentina, March 1994

BLG 647

PRESSURE VESSEL STEEL RESEARCH: BELGIAN ACTIVITIES

E. van Walle, A. Fabry, H. Aït Abderrahim, R. Chaouadi, P. D'hondt, J.L. Puzzolante, J. Van de Velde and T. Van Ransbeeck

SCK•CEN, Mol, Belgium

R. Gerard

Tractebel, Brussels, Belgium

IAEA Specialists Meeting on Advanced Structural Integrity Assessment Procedures

Argentina, March 1994

BLG 647

Pressure Vessel Steel Research: Belgian Activities

E. van Walle, A. Fabry, H. Aït Abderrahim, R. Chaouadi, P. D'hondt, J.L. Puzzolante, J. Van de Velde and T. Van Ransbeeck
SCK•CEN, Boeretang 200, B-2400 Mol, Belgium

R. Gerard
Tractebel Energy Engineering, Avenue Ariane 7, B-1200 Brussels, Belgium

Abstract: A review of the Belgian Research Activities on Nuclear Reactor Pressure Vessel Steels and on related Neutron Dosimetry Aspects is presented. Born out of the surveillance programmes of the Belgian NPP's, this research leads to the development of material-saving techniques, like reconstitution and miniaturisation, and to improved neutron dosimetry techniques. A physically-justified RPVS fracture toughness indexation methodology, supported by micro-mechanistic modelling, is based on the elaborate use of the instrumented Charpy impact signal. Computational tools for neutron dosimetry allow to reduce the uncertainties on surveillance capsule fluences significantly.

Keywords: reactor pressure vessel steel, neutron dosimetry, neutron transport calculations, fracture toughness indexation, instrumented Charpy-V impact, reconstitution, miniaturisation, plant life management, fracture mechanics

1. Introduction

The seven pressurised water reactor plants, operated in Belgium by the utility ELECTRABEL, represent a total capacity of more than 5500 MW. In 1993, they assured the production of 60% of the country's electricity. The main characteristics of these units and the status of their pressure vessel surveillance programmes are summarised in Table 1. All surveillance capsules retrieved are tested at SCK•CEN, the Belgian Nuclear Centre.

Plant	Capacity MWe	First operation	Number of capsules	Capsules withdrawn
Doel 1	400	1974	6	3 (1977,80,89,93)
Doel 2	400	1975	6	4 (1977,82,82,91)
Doel 3	975	1982	6 (*)	2 (1986,88)
Doel 4	1010	1985	6 (*)	1 (1989,94)
Tihange 1	870	1975	8	3 (1979,85,92)
Tihange 2	900	1983	6 (*)	2 (1986,89)
Tihange 3	1020	1985	6 (*)	1 (1988)

(*) 4 capsules in the reactor vessel and 2 in standby for delayed insertion

Table 1: The Belgian nuclear units and the status of their surveillance programme

The test matrix within these capsules scopes the future embrittlement status of the reactor pressure vessel. The actual information on the vessel embrittlement, evaluated according to nationally accepted regulations and standards, indicates that the embrittlement of the vessels should remain acceptable largely beyond 40 years of operation. As a consequence, a modified withdrawal scheme for the remaining capsules in the Belgian NPP has been adopted. This schedule allows to investigate the embrittlement status up to 50 or 60 years of operation.

On the research side, the shortage of vintage material for the older plants and the interest to revisit some destructively tested materials, called for optimised use of the material stock. Besides opening a vast area for development - from reconstitution to miniaturisation - the information from classical tests has to be maximised, promising test techniques have to be evaluated and correlations with the classical tests have to be established. As will be shown, this approach could lead to an extended surveillance methodology where non-arbitrary indexation parameters are used to evaluate the embrittlement of the reactor pressure vessel material. This methodology is complemented by the development of physical models of embrittlement and validated on test results on reference reactor pressure vessel steels (RPVS), to come to relevant fracture toughness indexation procedures. The need to understand the apparent outlier behaviour of the Doel 1&2 reactor pressure vessel welds[1], has provided the initial impetus for this research program.

A special effort is also devoted to improve the neutron dosimetry techniques and to validate the computational tools, used to assess the fast neutron fluence at the inner surface of the pressure vessels. In this frame, many benchmark experiments were conducted in the VENUS critical facility and the BR1-reactor at SCK•CEN.

These developments are financially supported by the utility ELECTRABEL. In order to have access to the international community, SCK•CEN and TRACTEBEL participate in several Round-Robins and play an important role in international committees, like: AMES, ASTM, CSNI, ESIS, EWGRD, IAEA and WGRD-VVER. Moreover, co-operation programmes with universities, research institutes and official organisations in the domains of interest, are established.

2. The Pressure Vessel Surveillance Programme

The pressure vessel surveillance programme of the Belgian NPP was designed according to ASTM-procedure E185 and is, besides some slight modifications, executed according to E185.

2.1. The capsules

The reactor surveillance capsules are placed in the beltline region towards the inner surface of the nuclear reactor vessel, with a typical lead factor varying between 2 and 3. Every capsule contains Charpy-V bars, tensile specimens and fracture mechanics samples, prepared from base, weld and heat affected zone materials, representative for the actual vessel. The heat treatment is representative of the one for the beltline material.
Various radiometric neutron dosimeters and fissile detectors (Fe, Ni, Cu, Ti, Nb, depleted U and Np), as well as temperature monitors are inserted at selected positions into the capsule.
At the time of the vessel fabrication, reference 'baseline' tests were made on similar non-irradiated specimens.

2.2. Information from RPV capsules

The capsule is dismantled at the LHMA hot cells of SCK•CEN. Visual inspection of the low melting point eutectic temperature monitors tells whether the upper temperature limit has been exceeded, but gives no information on the excess time nor on the lowest temperature during irradiation.
The radiometric neutron dosimeters are counted with Ge γ-spectrometry installations, calibrated in efficiency and energy, whereas to deduce the absolute specific activity of these dosimeters. The fissile detectors, as initially mounted, are put in solution and subsequently a selected fission product activity (^{137}Cs, ^{134}Cs or ^{106}Ru) is counted with the γ-installation. These specific activities are then used to derive the saturated activities by taking different parameters into account, such as: the reactor power history during the irradiation and the decay during the irradiation, the cooling time and the measurement. From the saturated activities, the fast neutron fluence (E > 1 MeV) received by the samples, is derived by using the cross-section above 1 MeV, averaged on the local spectrum deduced from transport calculations. These neutron transport calculations - based on the S_n-method (the LEPRICON-code, used at SCK•CEN) or on the Monte-Carlo method (the MCBEND-code, used at TRACTEBEL) - allow to relate the surveillance capsule neutron dose to the actual vessel condition (inner surface, 1/4 T, ...).

Tensile testing, primarily according to ASTM E8, is performed at reactor operating temperature, yielding the stress-strain curve of the irradiated vessel material. Instrumented Charpy-V impact tests, for the non-instrumented part according to ASTM E23, are performed as a function of temperature, to obtain the brittle-ductile transition curve of the irradiated materials. The compact tension fracture mechanics specimens have not been tested until now, as no requirement exists from the regulatory side.
In general, neutron exposure of vessel material induces an increase in hardness and other strength properties, and reduces the ductility of the material. These properties are commonly detected: in tensile specimens as an increase in tensile strength, while fracture occurs at lower strain values; in the Charpy test: the strength increase is seen

as a shift in temperature of the Charpy-V energy curve as a function of temperature, combined with a lowering of the maximum energy needed to break a fully ductile specimen (upper shelf energy, USE). This is illustrated by the top part of Figure 1. The Charpy impact test gives also information on the lateral expansion of the broken sample (LE) and the percentage of crystallinity of the fracture surface (also expressed by its complement: the shear fracture appearance (SFA)). The functional dependence on temperature is similar to the one for fracture energy: both LE and SFA shift after irradiation.

For Belgium, the vessel surveillance and integrity evaluation is mainly in accordance to the US Nuclear Regulatory requirements.
For the Charpy-V impact energy curve, the temperature shift of the brittle-ductile transition curve after irradiation, ΔT_{41J}, is indexed at 41J. Similar temperature shifts, $\Delta T_{.89mm}$, respectively $\Delta T_{50\%}$, are indexed at LE=.89mm for the lateral expansion curves, respectively at SFA=50% for the shear fracture appearance.
The temperature shift at 41J, an arbitrary conventional 'measure' for the embrittlement of the vessel material, is used to update the Reference Temperature of Nil Ductility Transition (RTNDT). The initial RTNDT for the unirradiated vessel material under consideration is defined according to ASME Section III: it results from a combination of drop weight and Charpy tests on unirradiated pressure vessel material.
The updated RTNDT, resulting from the surveillance tests, gives the basic ingredient to shift the lower bound fracture toughness crack initiation and arrest curves, as originally calculated in an empirical way from the ASME XI code. The overall method is demonstrated in Figure 1. The updated fracture toughness curves are then further used for the safety analysis of the reactor vessel. As for now, no Regulatory requirement on the direct measurement of fracture toughness curves exists, as long as the RTNDT does not exceed the PTS screening criterion and the C_V-USE is not less than 68J.
On the other hand, predictive formula allow to estimate the upper bound shift of the RTNDT. Here TRACTEBEL has, for the newer plants, adopted the French FIS-formula [2]. Figure 2 illustrates the measured RTNDT shifts from the Belgian surveillance programmes versus the shifts calculated with the FIS-formula.
Another surveillance programme result is the USE. Here the 10CFR50 Appendix G requires the initial USE of the vessel materials to be not less than 102J and requires the USE to be not less than 68J throughout the vessel lifetime.

3. The Research Programme

The surveillance programmes need to be backed by research in order to verify and to understand irregularities, observed in testing the capsule material. Uncertainties can stem from a variety of causes, like dosimetry evaluation, irradiation temperature, number of specimens (statistics), representativeness and orientation of the specimens. More fundamentally, the test techniques used in the surveillance programme can be questioned and - as indicated above - the toughness indexation methods applied, although conservative, are arbitrary.

This leads to a more general research programme concentrating on the development, correlation and justification of improved experimental techniques and theoretical models for evaluating the in-service behaviour of RPV Steels.
A basic reference for this research will be the reactor surveillance material of the 7 nuclear pressure vessels of the Belgian PWR's, conventionally tested to meet the current Regulatory requirements relative to the vessel fracture toughness. The ability to use minimum amounts of crucial material is a central issue from the beginning, which did lead to a documented elaboration of the technique of Charpy-V reconstitution and miniaturisation, qualified on reference steels in different material conditions. A thrust of these developments is the determination of irradiation-induced shifts using pre-cracked C_V-size specimens for fracture toughness evaluation. In parallel, full advantage is taken from all data generated from quasi-conventional surveillance tests: in particular, the instrumented Charpy-V traces and the Shear Fracture Appearance data, are interpreted in terms of a Charpy-V indexation procedure, based on the evolution of the load diagram of the material.
These mechanical test results are supplemented with micro-structural information to allow for an overall interpretation at light of physical models of embrittlement.

All the mechanical test results must be linked with the neutron dosimetry results in order to correlate the embrittlement with the irradiation. As the dosimetry results depend on neutron transport calculations, it is necessary to validate these tools on the basis of well-established benchmark experiments. Indeed, different parameters can affect the correct prediction capability of these calculation tools for the fast fluence on the RPV. Amongst them are: the fission spectrum, the neutron source distribution (especially in the core periphery), the geometrical model, the materials cross-section library and the cross-section dosimetry file. SCK•CEN and TRACTEBEL investigate these problems since many years and continue to improve their methodologies for predicting as accurately as possible, the fast neutron fluence integrated in the pressure vessel.

3.1. The Reconstitution Technique

SCK•CEN has developed a stud welding technique to reconstitute broken Charpy specimens [3,4,5]. The impetus for the development lay in the need to investigate the weld part of heat-affected-zone specimens of the Doel 1&2 power plants; unusually high copper content was detected in such specimens, as compared to the inventory of normal weld samples. The method, schematically illustrated in Figure 3, has been qualified extensively on various pressure vessel materials in non-irradiated and irradiated conditions, leading to acceptance by the Belgian authorities. The principle consists of welding two studs to an insert made of pressure vessel material, with subsequent remachining into a 'new' specimen. For now, two geometries are commonly prepared: a 10x10x55mm Charpy bar and a small tensile specimen of gage length 20mm and diameter 3.6mm. Proper choice of insert lengths allows to increase the statistics, i.e. the number of test samples made of representative material, by at least a factor of 3.

To avoid influences of the welding procedure on the inserts, reconstitution weldments are carried out on dummy specimens - loaded with a thermocouple that measures the temperature at 4mm from the weld interface - before and after reconstituting the inserts of interest. At all times the temperature has to remain below the normal operating temperature of the plant, i.e. 300°C.
The qualification tests give confidence that the reconstitution technique is properly designed in order to avoid any biases with the original specimens. Detailed finite element calculations to simulate the differences between as-received and reconstituted specimens, are in progress.
SCK•CEN plays a major role in the ASTM Round Robin on Reconstitution, designed to update ASTM guideline E-1253 on Reconstitution of Charpy-V bars.

3.1.1. Charpy-V impact specimens

The original qualification tests were executed on 20mm inserts. No deviation in energy, lateral expansion and shear fracture appearance between as-received and reconstituted Charpy-V impact tests were observed. However, to maximise the available amount of material, the insert length should be minimised. An interesting insert size is 10x10x10mm since it allows to reorient a Charpy sample - for example: from L-T to T-L - see Figure 4. However, for smaller insert length, the impact test reveals that, from a certain test temperature on, the plastic flow is constrained by the welds. Indeed, these weldments are situated at less than 5mm from the sample notch, while hardness testing on broken as-received specimens suggests that, at upper shelf test temperatures, the plastic flow can spread 8 to 10mm from the notch. Consequently, the loss in plastic flow energy causes the recorded fracture energy to be less than for an as-received sample. Initial two-dimensional finite element calculations confirm this behaviour. Figure 5 shows the energy reduction for unirradiated HSST-03 material in the L-T and T-L orientation. The apparent shift in temperature after reconstitution is - on Figure 5 - primarily a direct consequence of the lower USE.
Similar losses occur on the lateral expansion of the reconstituted 10mm inserts. On the other hand, as can be seen in Figure 6, the shear fracture appearance is independent of the reconstitution and, in the HSST-03 case, of the sample orientation. The shear fracture appearance gives information on a localised region, i.e. the fracture plane under the notch. The lateral expansion and fracture energy depend on the volume surrounding the notch, a volume restrained by the weldments.
For some steels, like some 22NiMoCr37 nuclear grade materials, there exists a lateral shift in temperature between the L-T and T-L transition curves of as-received samples. This shift depends on material properties and is also reflected after reconstitution.

Another source for energy differences with small inserts comes from the impact hammer geometry - DIN or ASTM - used for breaking the samples [4,5]. The edgy ASTM tup can introduce a Brinell type of deformation on the impact side of as-received samples and spends energy with this process. However, with reconstituted samples made from small inserts, the hard weld zones will interact with the ASTM-tup and the Brinell deformation disappears. Consequently an additional reduction in the fracture

energy is detected. The smooth round DIN-tup does not suffer from this effect as the considered Brinell deformation is not introduced on as-received or reconstituted samples. The combined effect of plastic flow constraint and hammer influence on the Charpy energy of 22NiMoCr37 steel is shown in Figure 7. The hammer effect is material dependent: it is less apparent for HSST-03, where losses mainly come from plastic constraint. In fact, the shape of the instrumented Charpy-V load-time curve and the inspection of the broken Charpy halves reveal whether the hammer effect is present [4,5].
The SFA for the tests on 22NiMoCr37 - illustrated in Figure 8 - is, however, again independent of the impact hammer used, sustaining the above statement that the shear fracture appearance gives information on what happens in a localised region, i.e. the fracture plane under the notch.

A regulatory requirement is to have Charpy results on weak T-L oriented specimens. With only L-T specimens available, the T-L as-received energy cannot be derived by simply testing L-T→T-L reconstituted specimens; one needs to test L-T→L-T reconstitutions too. The conceptual approach to find the T-L as-received energy was tested for HSST-03 and is illustrated in Figure 9. Considering the losses due to plastic constraint and to the hammer as isotropic, the difference in energy between the L-T as-received and the L-T reconstituted curves can be added to the experimentally determined T-L reconstituted curve; this leads to a predicted T-L 'as-received' curve, in excellent agreement with the experimentally determined one.
The application of the reconstitution technique of 10mm long inserts to materials with different upper shelf energy revealed that the maximum losses, recorded after testing at upper shelf temperatures, depend on the upper shelf energy of the samples. This is illustrated in Figure 10, where the spline fits through the experimental - non-irradiated, as well as, irradiated - data serve as a guide to the trends. Two further effects catch the eye: i) energy losses can depend on the hammer geometry and on the material; ii) there is a threshold USE below which no losses, due to the reconstitution of 10mm inserts, occur. The curves of Figure 10 prove that the losses can depend on the orientation of the material and this complicates the application of the simple correction method described above (Figure 9).
For some radioactive steels tested many years ago, an additional embrittlement (parallel temperature shift of the transition curve to higher temperature) was detected after testing reconstituted specimens (insert length of 20mm: no plastic constraint effects, therefore no reduction of the USE). A batch of the same radioactive C_V-samples was recently tested and subsequently reconstituted at VTT, Finland and SCK•CEN: after testing, no additional embrittlement was detected. The origin of the effect on the delayed reconstitution of those steels is probably material bound but remains up-to-now unclear.

In conclusion, it can be stated that the C_V-reconstitution of small insert lengths, influences the fracture energy and lateral expansion behaviour, but does not affect the SFA. The reduction in USE and the induced apparent shift in temperature at 41J are conservative from the safety viewpoint. There is tup geometry dependence on the USE and

the LE, but none on the SFA. The invariance of the SFA is advantageous in the frame of a new indexation methodology, to be highlighted in paragraph 3.3.

3.1.2. Precracked Charpy-V specimens

Precracking and side-grooving Charpy-V specimens leads essentially to plane strain conditions in the notch plane. Three point bend tests on these samples act on the material concentrated in the notch plane. Reconstitution should therefore be possible with small insert lengths without influencing the results.
J_{Ic}-compliance tests were conducted on as-received and reconstituted samples (10mm inserts) at upper shelf temperatures (most stringent condition) in collaboration with Nuclear Electric, Berkeley, UK. The deduced J_{Ic}-values are identical.
Although Charpy-V specimens do not fulfil the ASTM size requirements for direct K_{Ic} measurements, the 3PB-results can be used for relative comparison of fracture toughness values and can be the basis for a more physically-grounded fracture toughness indexation procedure of the embrittlement of RPVS. This is the current topic of a demonstration experiment co-operatively undertaken by SCK, ORNL and VTT. This collaboration looks for correlations between K-values from Charpy size specimens and CT size samples (up to 4T-CT), made of an irradiated US reference weld.

3.1.3. Tensile specimens

Mini tensile specimens were reconstituted from Charpy remnants of 22mm in length [6,7]. The gage length-to-diameter ratio of the reduced part was identical to the ratio for the ASTM E8 defined Pin-Loaded Tension Test Specimen with 2 inch gage length; the latter specimen is present in the surveillance capsules. Qualification tests on as-received and reconstituted mini-tensile specimens, together with tensile tests on the E8 specimen size were conducted. This resulted in a one-to-one correspondence for the tensile properties of all specimens. As an application, Doel 2 weld unirradiated reference Charpy halves were reconstituted and tested at reactor operation temperature, to determine the baseline tensile properties. The results can be found on Figure 22 in Section 3.4.2..
In the near future, we will reduce the insert length down to ~10mm in order to prepare notched precracked tensile specimens for direct toughness evaluation. Again, quasi plane-strain conditions will reduce the plastic deformation. Moreover, the notch eliminates the risk of rupture out of the region of interest. Comparative tests with non-reconstituted tensile specimens will be carried out as well (see 3.4.1.).

3.2. Miniaturization of Charpy-V specimens

Miniaturized Charpy-V specimens are an alternative for optimising the use of surveillance material. Moreover, in special situations, like e.g. scoping an operational reactor vessel through boat sampling, the maximum size of the specimens is limited. Actually, some interest goes to the DIN50115 standard specimen with dimensions 3x4x27mm. Validation of these specimens requires correlations with data obtained from the standard 10x10x55mm specimens.

The toughness behaviour of these small specimens (MS) has been characterised by several authors [8,9] with index temperatures like $T_{1.9J}$, $T_{3.1J}$, $T_{0.3mm}$ [8], respectively corresponding to the empirical indices T_{41J}, T_{68J}, $T_{0.9mm}$ of the standard 10x10x55mm size specimens (SS). This leads to a seemingly simple empirical formula, $T_{SS}=T_{MS}$ + 70K, the mean correlation of a rather large data base whose scatter band [8] is shown in Figure 11.
Mini-Charpy specimens of Doel 4 base and weld material, prepared with the electric discharge technique, were tested with instrumented equipment to verify the scatter of mini specimens and to check the proposed correlation. As can be estimated from Figure 12, the scatter of the mini-Charpy impact results turns out to be comparable to the scatter for the standard size specimen. The correlation result for the Doel 4 base material is within the scatter band of Figure 11. However, although the temperature shift of the energy curves indexed at 1.9J and 41J is only 33K and although the lateral expansion gives a similar result, the shift indexed at 50% shear (for both geometries) corresponds to about 78K - as illustrated in Figure 12.
Consequently, caution should be taken to introduce empirical indexation shifts with large error bars (moreover, the initial indexation is already empirical). The indexation approach should take information from the instrumented signal on mini and standard specimens, combined with the physical differences between the two geometries, like volume effects and strain rates - as illustrated on Figures 11 and 12 - into account [10].
From an experimental viewpoint, it should be mentioned that the thermal mass of mini C_V-specimens is much lower than for standard C_V-specimens. The specimen transit times from thermal bath to impact should therefore be drastically reduced. SCK•CEN co-developed a mini C_V impact system where the standard 5 second transit-time is reduced to below 2 seconds.

3.3. Interpretation of the instrumented Charpy-V impact signal

The classic general principles of RPVS embrittlement modelling in the ductile-brittle transition temperature range are summarised on Figure 13. To first approximation, the ductile-brittle transition temperature (DBTT) can be considered as the temperature corresponding to the intersection between the general yield curve and the micro-cleavage fracture stress. Irradiation does, generally, not affect the micro-cleavage fracture stress, but raises the general yield curve. This leads to the so-called DBTT shift, a measure for RPVS embrittlement. In surveillance capsule programmes, this shift is by contrast taken at an arbitrary level of absorbed energy (e.g. 41J).
The ideas, presented below, are summarised from a recent paper[10].

Charpy impact machines, instrumented with strain gages, measure - as a function of time t - the load P exerted by the impacting tup on the Charpy sample. The (P,t) Charpy impact curve can contain, depending upon the test parameters, several characteristic load points: P_{GY}, the general yield load; P_m, the maximum load; P_u, the brittle crack initiation load; P_a, the crack arrest load[11].
For our analysis purposes, the instrumented signal is subdivided in several parts, schematically illustrated in Figure 14. Three or four critical temperatures and a related

energy partitioning can experimentally be determined to reasonable accuracy from the impact traces [10], [12-14]:

T_D: 'brittleness' temperature = the onset of 'energy fraction A'. Above this temperature, plastic deformation of the sample is necessary to cause fracture.

T_I: ductile crack initiation temperature = the onset of ductile crack growth, i.e. the temperature at which the SFA starts to exceed 0%.

T_N: 'ductility' temperature = the onset of 'energy fraction B'. In the transition region, this ductile tearing can suddenly change to unstable brittle crack propagation (point 'u' on the impact trace).

T_0: the onset of the Cv upper shelf, i.e. the temperature at which brittle crack initiation and crack arrest loads coincide; at higher temperature, inflexion of the velocity-time record allows to define the shelf of 'energy fraction C'.

At high strain rates, such as in the C_V-test, T_D is generally close to T_I.

Energy fraction B contains mainly plastic deformation energy, but 'measures' also the specimen's capability to sustain stable ductile crack growth; most of the scatter in the transition region for the C_V-test is associated to this fraction. Conversion from ductile to brittle behaviour stems from the interaction with 'trigger' particles under the strain field triaxiality, prevailing in conventional Charpy-V specimens. Upon irradiation, fraction B diminishes drastically: the reduction in ductility favours the conversion to brittle behaviour and reduces the statistical variation. Fraction C indicates the ability to stop a fast crack and to return to the tearing mode, but under plane stress conditions, characterised by shear lip formation.

Energy transition curves are a superposition of the individual fits of the energy fractions A, B and C; this explains their slightly unusual shapes (Figure 15).

Comparison of energy transition curves of non-irradiated and irradiated surveillance samples with subsequent indexation at an arbitrary energy level in the transition region (like 41J), can lead to surprising results: whereas in the non-irradiated data the transition region can, for example, be controlled by fraction A, some contribution of fraction C may be needed in the irradiated condition in order to reach 41J (due to the fact that fraction A and B are reduced through irradiation). This feature is demonstrated in Figure 15. The regulatory indexation at the 41J level can in such cases lead to an unrealistically large shift, for which no explanation can be found when using the classical hyperbolic tangent fit of the total Charpy-V energy. The apparent outlier behaviour results from the fact that the 41J shift depends on the relative position of the shelf and transition temperature of the various fractions in the baseline and irradiated condition. This indexation bias can be different from material to material and depends on the irradiation level.

Not only can energy shifts misleadingly correlate different physical phases within the fracture of C_V-specimens, but they can also be influenced by the reconstitution technique, a cornerstone for future plant life management. The unravelling of these artefacts encourages the search for other indexation parameters. The load diagram as a function of temperature, Figure 14, is the more adequate reference for indexation. Especially T_I and T_0 are physically-grounded measures of the DBTT: T_0 is directly correlated to the transition temperature TT_C of the corresponding energy fraction, taken at 50% of its shelf.

Figure 16 shows, as an example, the instrumented C_V-impact load diagram and SFA for the Doel 4 base material. As is apparent, there exists a one-to-one correlation between the C_V-impact load diagram and the shear fracture appearance, bound by the two characteristic temperatures T_I and T_0. A fit of the experimental SFA-data can be derived from the load diagram as

$$SFA\ (\%) = [1 - (P_u - P_a)/(P_m + k(P_m - P_{GY}))] \times 100\%$$

where, $0.4 \leq k \leq 0.6$ [10]. Most tests show that k=0.5 tends to be a good approximation of reality. This method allows for an excellent correspondence with the experimental SFA-results.

An example of the evolution of the load diagram after irradiation is shown in Figure 17. The unique relationship between the SFA-data and the respective load diagrams is depicted for the baseline and irradiated condition. The shift of the load diagram between the baseline and irradiated condition, reflected by the shift of T_I and T_0, corresponds in this case to the SFA-shift at 50% shear. Most importantly, Figure 17 is a direct experimental expression of the Davidenkov diagram of Figure 13: it establishes the relationship between hardening and DBTT-shift of the steel (shift of T_I, T_0), bringing also together the static and dynamic yield stresses; in turn, this provides input needed for [10]: i) the modelling of embrittlement mechanisms and ii) the micro-mechanics-based correlation of fracture toughness shifts.
Another interesting feature of the load diagram is the independence to reconstitution and to the hammer geometry. These effects are illustrated in Figure 18 for the reconstitution of 10mm long inserts of HSST-03 material and more general in Figure 19 for different data on the 22NiMoCr37-material.
In conclusion, elaborate use of the instrumented C_V-signal brings new insight into the embrittlement of RPV Steels, and in particular allows improved indexation of dynamic fracture toughness K_{Id} through physically meaningful temperatures T_I and T_0 characterising the load diagram.

3.4. Damage modelling

3.4.1. Micro-mechanics using local approach

The local approach looks at the evolution of microscopic behaviour to derive macroscopic quantities. The evolution of damage towards macroscopic crack initiation depends on the initial damage model adopted. This model describes the microscopic mechanisms that induce fracture.
In order to describe the damage evolution, the local stress-strain history of the material has to be computed through finite element calculations. The combination of the stress-strain history with the damage model allows to determine the critical damage needed for crack initiation.
A simple cylindrical tensile geometry with various notches was chosen to verify the proposed models. This geometry has the advantage that it is easy to simulate with two-

dimensional finite element calculus, that the loading condition could be easily modified by simply changing the notch radius and that the experiments are straightforward tensile tests.
Two micro-mechanically-based ductile damage models have been applied to two reactor pressure vessel steels, namely 18MND5 (at 20°C) and 22NiMoCr37 (at 100°C). The comparison of experimental results to finite element calculations shows an overall good agreement, as illustrated in Figure 20. Physically, ductile fracture is related to the nucleation, growth and coalescence of cavities created around second phase particles. Thus, the Rice and Tracey void enlargement model and the damage work associated to plastic flow and cavity growth have been used as damage models [15]. The local damage model is given in its general form as:

$$\dot{D} = f(\sigma_{ij}, \dot{\varepsilon}^{p}_{ij}, \alpha_{k})$$

where $\dot{D}$ is the damage rate, σ_{ij} are the stresses, $\dot{\varepsilon}^{p}_{ij}$ are the plastic strain increment and α_k are the parameters of the model. The evolution of both models with mean strain as well as the crack initiation level are given in Figure 21. For both investigated materials and models, the critical value, D_c - associated to crack initiation - is geometry independent and thus could be considered as a material constant. The most severe condition to test these damage models would be the crack tip condition. Tests on precracked Charpy specimens in three-point bending have been carried out using the unloading compliance technique. The finite element simulation as well as the application of these damage models are still in progress. In the near future, we intend to test radioactive reference materials to verify correlations with other techniques mentioned throughout this paper.

3.4.2. Damage modelling and micro-structural characterisation

Our damage modelling effort can best be summarised by starting with the Davidenkov diagram of Figure 13, experimentally transposed into load diagrams such as the ones of Figure 17. If the microscopic fracture stress is found invariant upon service exposure, embrittlement is represented in terms of *hardening* damage mechanisms alone, i.e. irrespective of whether or not grain or lath boundaries are weakened by segregations; indeed, interfacial coverage sufficient to promote intergranular fracture would also measurably decrease this fracture stress. Furthermore, and as needed, confirmation is independently provided through SEM examination of the fracture surfaces. In our work, hardening stemming from copper precipitation effects is described in first approximation by the Fisher model[16], and we concentrate on the deviations of the experimental data from these initial "predictions". A first type of deviation entails the distinction between bulk copper content of the steel and copper in solid solution within the matrix: copper precipitated during the steel heat treatment or chemically bound (e.g. as sulphide) does not contribute to irradiation embrittlement. An example is given by the Doel 1&2 Soudotenax welds[1]; this is illustrated by Figure 22 in terms of static yield stress increase: specimens with bulk copper contents of 0.15% and 0.37% cannot be distinguished, and follow a trend curve corresponding to the lower content. This is supported by extensive evaluation of reconstituted C_V-data[17] and is

presently under direct verification through high resolution field emission gun transmission electron microscopy[18]. But in general, the most important deviations from the Fisher model are due to the presence of *at least* two other, competing, hardening mechanisms, and our emphasis since the last few years has been to separate their influences. From a phenomenological viewpoint, this has been and continues to be done by examining data obtained at different irradiation temperatures, in combination with annealing studies. We follow an approach pioneered by Pachur[19]. In this sense, we have long identified[20] two mechanisms active at PWR temperatures, and labelled them mechanisms 2 and 2A: see an example on Figure 23; the second mechanism displays an incubation fluence function of alloying elements, most certainly nickel, and both depend on irradiation temperature. The micro-structural origin of the corresponding hardening obstacles is not yet fully clear, but our candidate explanations have led us to select two experimental techniques to help actual identification and more quantitative characterisation in terms of defendable engineering trend curves: positron annihilation lifetime spectroscopy[21] and mechanical spectroscopy, including internal friction[22]. It has been recently found that unexpected insight may also be gained from the combined C_V-tensile load diagrams, and this potential avenue is being explored further by dedicated tests.

3.5. Neutron dosimetry

3.5.1. In-vessel surveillance dosimetry

At the end of the seventies, the US Nuclear Regulatory Commission (NRC) established the Light Water Reactor Pressure Vessel Surveillance (LWR-PV-SDIP) to improve, maintain and standardise neutron dosimetry, damage correlations and the associated reactor analysis procedures used for predicting the integrated effect of neutron exposure to LWR-PV. Four principal laboratories collaborated in the conduct of this program: HEDL, Richland, Washington; NIST, Gaithersburg, Maryland; ORNL, Oak Ridge, Tennessee and SCK•CEN, Mol Belgium. Later on, other European laboratories - RR&A, Derby, UK; AEA, Winfrith, UK; and KFA, Jülich, FRG - joined the collaboration.

One of the major contributions of SCK•CEN to this program in the eighties, was the VENUS PWR Engineering Mock-Up Experiment, that was established as one of the benchmark fields to the LWR-PV-SDIP. The VENUS programme was sponsored by the Belgian Utilities. Its particularity is a precise modelling of a generic 3-loop power plant: indeed, its core loading was made of pins with the same diameter, similar ^{235}U-enrichment and the same pitch as the 17 x 17 fuel assemblies of modern PWR's. It had a staircase shaped core boundary with a steel baffle, a core barrel and a thermal shield with thicknesses and at distances from the core representative of the actual PWR's.

The program was conducted in three phases: VENUS-1 [23], representing a fresh core loading; VENUS-2 [24], representing a 'low-leakage' core loading; and VENUS-3 [25], simulating the Partial Length Shielded Assembly (PLSA) concept. In the three configurations, the investigated parameters were the pin-to-pin power distribution, the

propagation of the fast neutrons outside the core and the γ-dose rates in the steel structure. Figure 24, taken from reference [26], illustrates the improvement of the dosimetry results when the benchmarks are used to validate the adopted analysis procedures. Actually, in order to take advantage of the experimental and computed results of the VENUS-programme, an effort[27] is going on at SCK•CEN to bring these data into the benchmark data base of the LEPRICON code system, which is used to analyse the capsule surveillance dosimetry.

3.5.2. Ex-vessel dosimetry

In the frame of future plant life management, some utilities are interested in the use of ex-vessel dosimetry in order to monitor the vessel fluence. When using the same computational tools as for in-vessel dosimetry to analyse such ex-vessel dosimetry, a calculational overestimation in comparison with the experimental results, is observed. To investigate this trend, a 'Concrete Benchmark Experiment'[28] in the BR1-reactor at SCK•CEN, was implemented. The aim is to study the backscattering effect due to the presence of concrete, and to validate - on the basis of the experimental results of this experiment - the computational scheme used for ex-vessel dosimetry analysis. Actually, the analysis is in progress and the preliminary results are encouraging.
Latter study is conducted in collaboration with the French Utilities EDF.

3.5.3. Maintenance of the dosimetry expertise

To maintain the expertise gained over all the years of international collaboration, SCK •CEN is carrying on this policy. Actually, SCK•CEN is participating in international programmes, such as DAVIS-BESSE 1, dedicated to ex-vessel cavity dosimetry[29], and the KORPUS Benchmark Facility Characterisation, representing a VVER-1000 Mock-Up.

4. Conclusion

The Belgian Activities on Pressure Vessel Steel Research make elaborate use of the 'normal' surveillance programmes of the Belgian Nuclear power plants to develop an advanced research programme on the characterisation and modelling of Reactor Pressure Vessel Steels. The research activities question the actual arbitrary indexation methods for steel embrittlement, and put forward a methodology - based on the information contained in the instrumented Charpy-V signal - to come to physically based indexation procedures. On the technical side, advanced specimen preparation and analysis techniques make use of limited amount of material to optimise the use of the material stock available. In parallel, test techniques are being developed to measure fracture toughness directly or to get Charpy-V information from small specimen sizes. A continuous effort on neutron dosimetry techniques and computational tools to maintain the expertise is this domain, is conducted at SCK•CEN.

5. References

[1] Gerard R., Fabry A.
in 'Integrity Assessment of Doel 1 and Doel 2 Reactor Pressure Vessel', IAEA Specialist's Meeting on Integrity of Pressure Components of Reactor Systems, Paks, May 1992.

[2] van Walle E., Fabry A., Gerard R.
in 'National Perspectives on Irradiated Embrittlement and its Mitigation', IAEA TRS16, Chapter 14, to be published

[3] Langouche F., Chaouadi R., Puzzolante J.L., Vandermeulen W., Van de Velde J. Van Ransbeeck T.
in 'Qualification of Charpy Specimen Reconstitution Procedure for Unirradiated Specimens', SCK•CEN R2756, 1989.

Vandermeulen W., Fabry A., Puzzolante J.L., Van de Velde J., Van Ransbeeck Th. and van Walle E.
in 'Charpy Specimen Reconstitution as a Means of Providing Data for PLEX Licensing Purposes', Int. J. Press. Vessel and Piping 54, 1993, p. 89-98.

[4] van Walle E., Van Ransbeeck T., Chaouadi R., Fabry A., Puzzolante J.L., Vandermeulen W., Van de Velde J., Klausnitzer E., Gerscha M.
in 'The Reconstitution Effort at SCK•CEN', ASTM E10.02 Workshop on Reconstitution, San Diego, January 1991.

[5] van Walle E., Fabry A., Van Ransbeeck T., Puzzolante J.L., Vandermeulen W., Van de Velde J., Klausnitzer E., Gerscha M.
in 'The Reconstitution of Small Remnant Parts of Charpy-V Specimens', SMiRT 11, Post-Conference Seminar on 'Assuring Structural Integrity of Reactor Steel Pressure Boundary Components', Taipei, August 1991.

[6] van Walle E., Van Ransbeeck T., Fabry A., Puzzolante J.L., Vandermeulen W., Van de Velde J.
in 'Qualification of Reduced Reconstituted Tensile Specimens", SCK•CEN R2883, 1991.

[7] van Walle E., Van Ransbeeck T., Fabry A., Puzzolante J.L., Van de Velde J.
in 'Technical Report on Reconstituted Tensile Specimens of Cv specimen size', SCK•CEN R2892, 1991.

[8] Klausnitzer E., Kristof H., Leistner R.
in 'Assessment of Toughness Behavior of Low Alloy Steels by Subsize Impact Specimens', 8th Int. Conf. on Structural Mechanics in Reactor Technology, Brussels, August 1985.

[9] Kryukov A.
private communication

[10] Fabry A, van Walle E., Chaouadi R., Wannijn J.P., Verstrepen A., Puzzolante J.L., Van Ransbeeck Th., Van de Velde J and T. Petrova.
in 'RPV STEEL EMBRITTLEMENT: Damage modeling and micromechanics in an engineering perspective', paper presented at the IAEA/OECD Specialists Meeting on Irradiation Embrittlement and Optimization of Annealing, Paris, September 1993; to be published by IAEA.

[11] 'Proposed Standard Method for the Instrumented Charpy-V Impact Test on Metallic Materials', ESIS Technical Sub-Committee on Dynamic Testing at Intermediate Strain Rates, Draft January 1994.

[12] Wullaert R.A., Ireland D.R., Tetelman A.S.
in 'Radiation effects on the Metallurgical Fracture parameters and fracture toughness of Pressure Vessel Steels', ASTM STP 484, 1970, p. 20-39.

[13] Tetelman A.S., Mc Evely A.J.
in 'Fracture of Structural Materials', John Wiley&Sons, New York.

[14] Pachur D.
in 'Influence of Radiation Damage Mechanisms on the Load Signal and on the Transition Curve of Instrumented Impact Testing', J. Nucl. Materials 160, 1988, p. 24-33.

[15] Chaouadi R., De Meester P. and Vandermeulen W.
in 'Damage Work as Ductile Fracture Criterion', to be published in Int. J. Fracture.

[16] Fisher S.B. and Buswell J.T.
in 'A Model for PWR Pressure Vessel Embrittlement', Int. J. Press. Vessel and Piping, Vol. 27, 1987, p. 91-135.

[17] Gerard R., Fabry A., Van de Velde J. Puzzolante J.L., Verstrepen A., Van Ransbeeck Th., van Walle E.
in ' In-service Embrittlement of the Pressure Vessel Welds at the Doel 1 and 2 Nuclear Power Plants', to be presented at the 17th ASTM Symposium on Effects of Radiation on Materials, Sun Valley, June 1994

[18] Phythian W.J.
in 'Microstructural Assesment of Belgian Weld Material', AEA-TRS-2062, 1991.

[19] Pachur D.
in 'Radiation Annealing Mechanisms of Low-Alloy Reactor Pressure Vessel Steels Dependent on Irradiation Temperature and Neutron Fluence', Nucl. Technol. 59, 1982, p. 463.

[20] Fabry A., Van de Velde J.
in 'Embrittlement and Annealing Mechanisms of LWR Pressure Vessel Steels', IAEA Specialist's Meeting on 'Radiation Embrittlement on Nuclear Reactor Pressure Vessel Steels', Balatonfüred, September 1990.

[21] Vanhoorebeke L.
in 'Positron Annihilation Measurements on Nuclear Reactor Pressure Vessel Steels', paper to be presented at the Europhysics Industrial Workshop on 'Industrial Application of Positron Annihilation', March 1994.

[22] Van Ouytsel K.
Work in progress

[23] Fabry A. et al.
in 'Venus PWR Engineering Mock-up: Core Qualification, Neutron and Gamme Field Characterization', 5th STM-EURATOM Symposium on Reactor Dosimetry, Geesthacht, September 1984.

[24] Aït Abderrahim H. et al.
in 'Venus-2 PWR Engineering Mock-up: Core Qualification and Neutron Field Characterization', Physor 90, International Conference an the Physics of Reactors: Operation, Design and Computation, Marseille, April 1990.

[25] Maerker R.E. et al.
in 'Analysis of the VENUS-3 Experiments' 7th.ASTM-EURATOM Symposium on Reactor Dosimetry, Strasbourg, August 1990.

[26] Gold R. and Mc Elroy W.N.
in ' The Light Water Reactor Pressure Vessel Surveillance Dosimetry Improvement Program (LWR-PV-SDIP): Past Accomplishements, Recent Developments and Future Directions', Reactor Dosimetry: Methods, Applications and Standardization, ASTM STP1001, 1989.

[27] Aït Abderrahim H. et al.
in 'Analysis of the VENUS-1 Ex-Core Neutron Dosimetry using the LEPRICON code system', Reactor Dosimetry, ASTM STP1228, 1994.

[28] Aït Abderrahim H. et al.
in 'Concrete Benchmark Experiment, Ex-Vessel LWR Surveillance Dosimetry', Reactor Dosimetry ASTM STP1228, 1994.

[29] Carter G.S.
in 'Dosimetry Techniques and Methods Used to Obtain Reactor Cavity Dosimetry Benchmark Data for Vessel Fluence Analysis and Davis-Besse 1', 7th ASTM-EURATOM Symposium on Reactor Dosimetry, France, August 1990.

Fig. 1 REGULATORY INDEXATION OF FRACTURE TOUGHNESS

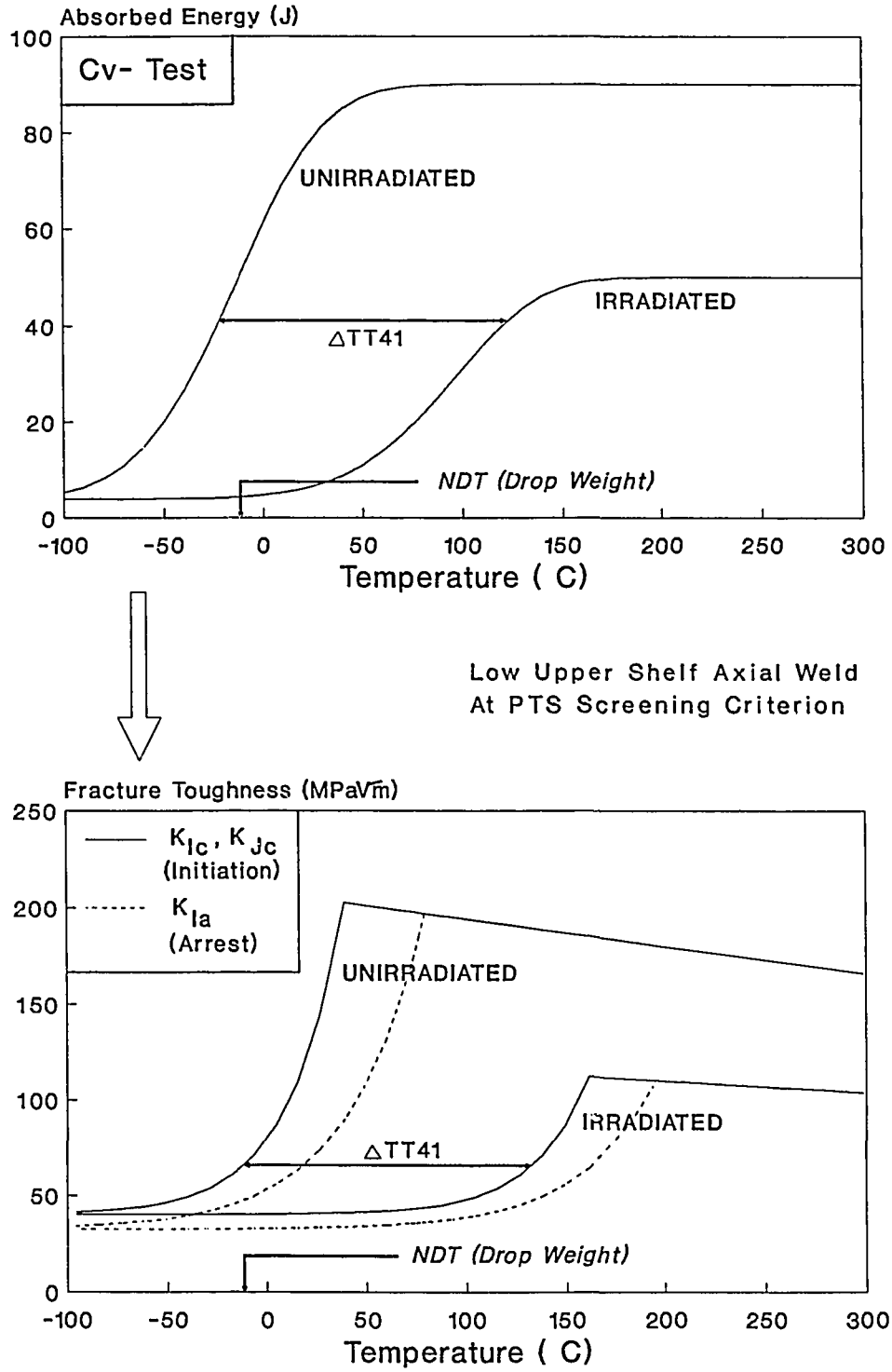

ASME Code Section XI Fracture Toughness Curves up to Upper Shelf

Fig. 2 MEASURED AND PREDICTED RTNDT SHIFTS FOR BELGIAN UNITS.

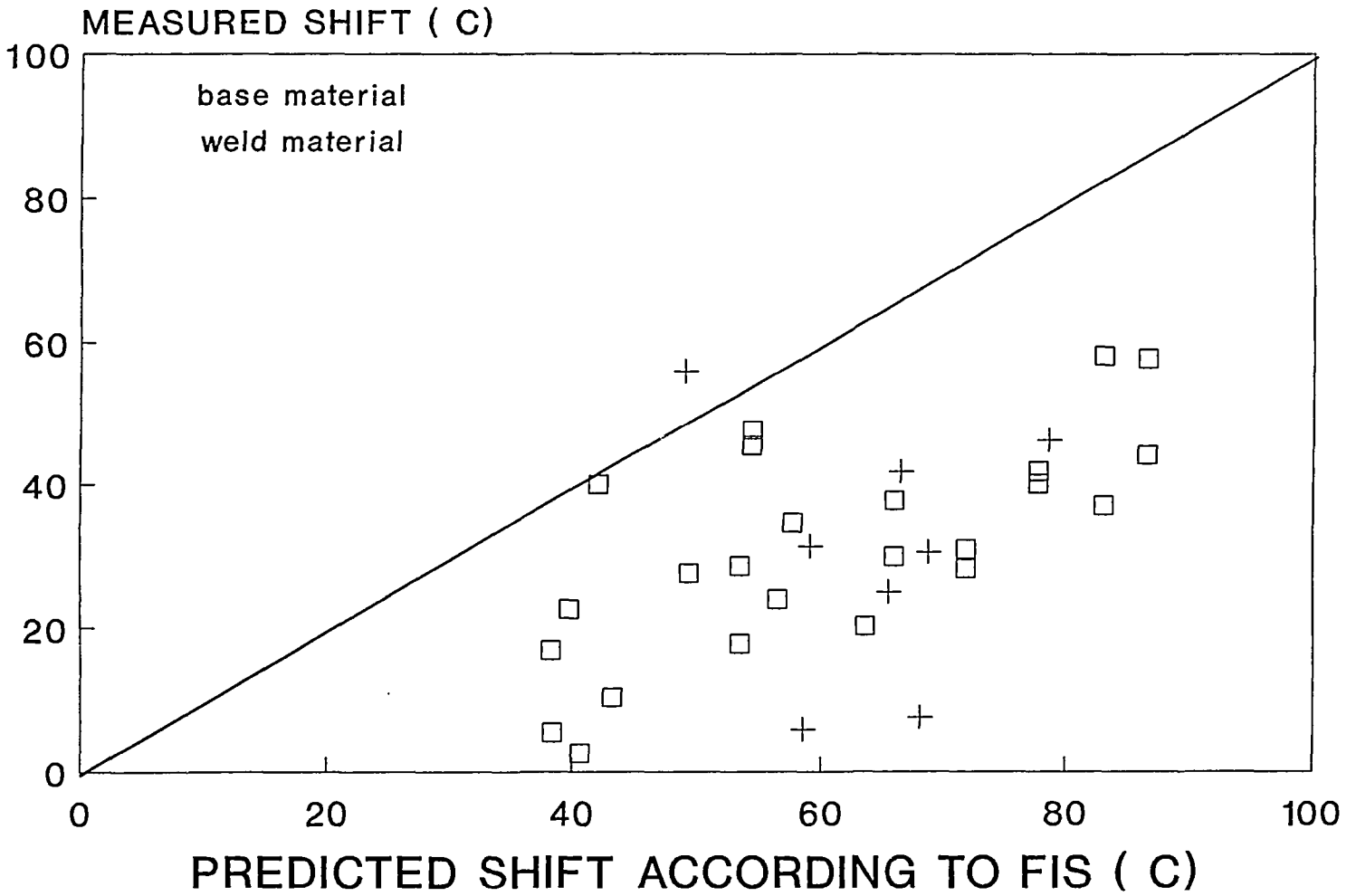

Fig. 3 SCHEMATIC PROCEDURE FOR THE RECONSTITUTION OF CHARPY SPECIMENS. THE INSERT LENGTH IS VARIABLE.

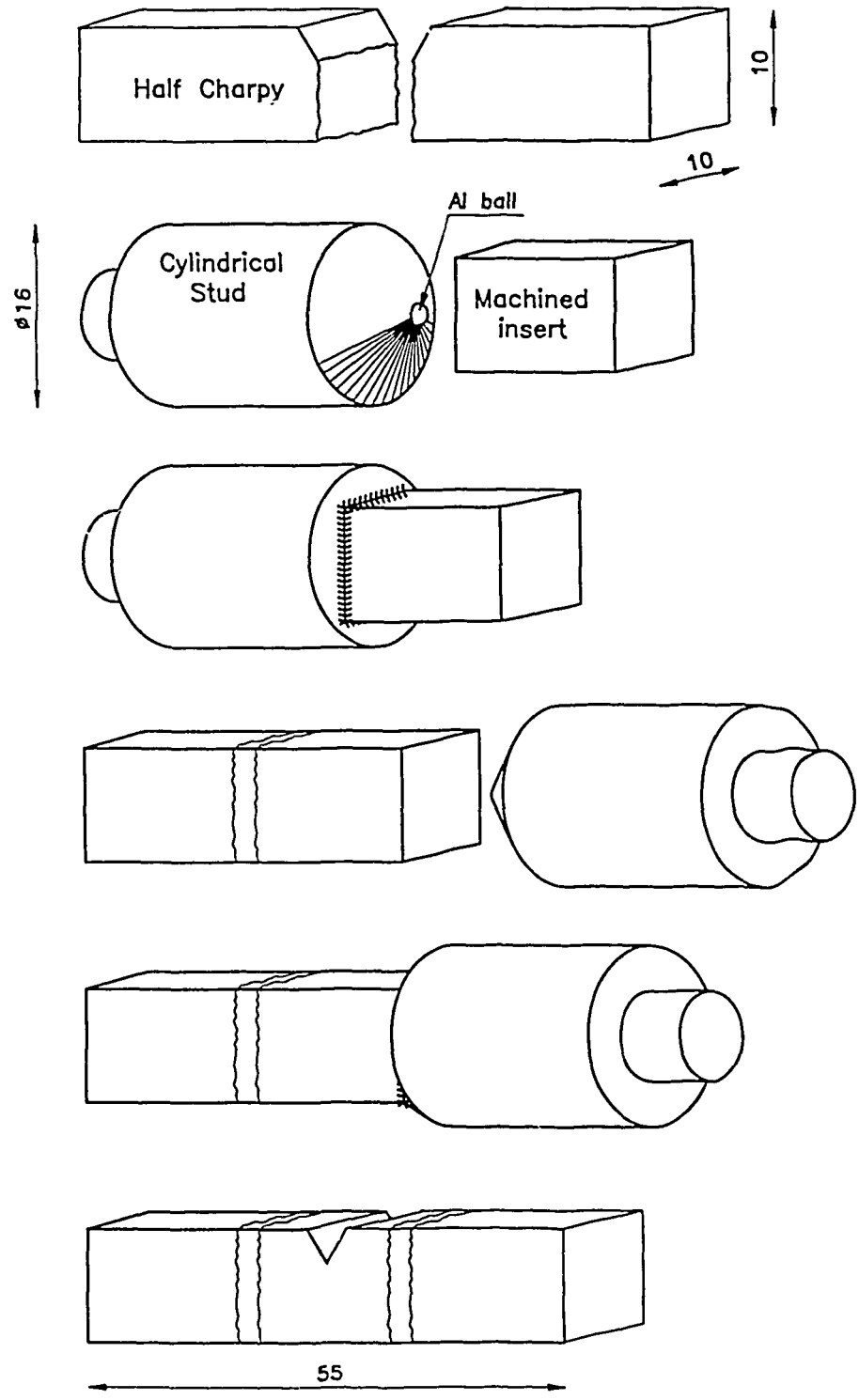

Fig. 4 THE RECONSTITUTION OF 10mm LONG INSERTS

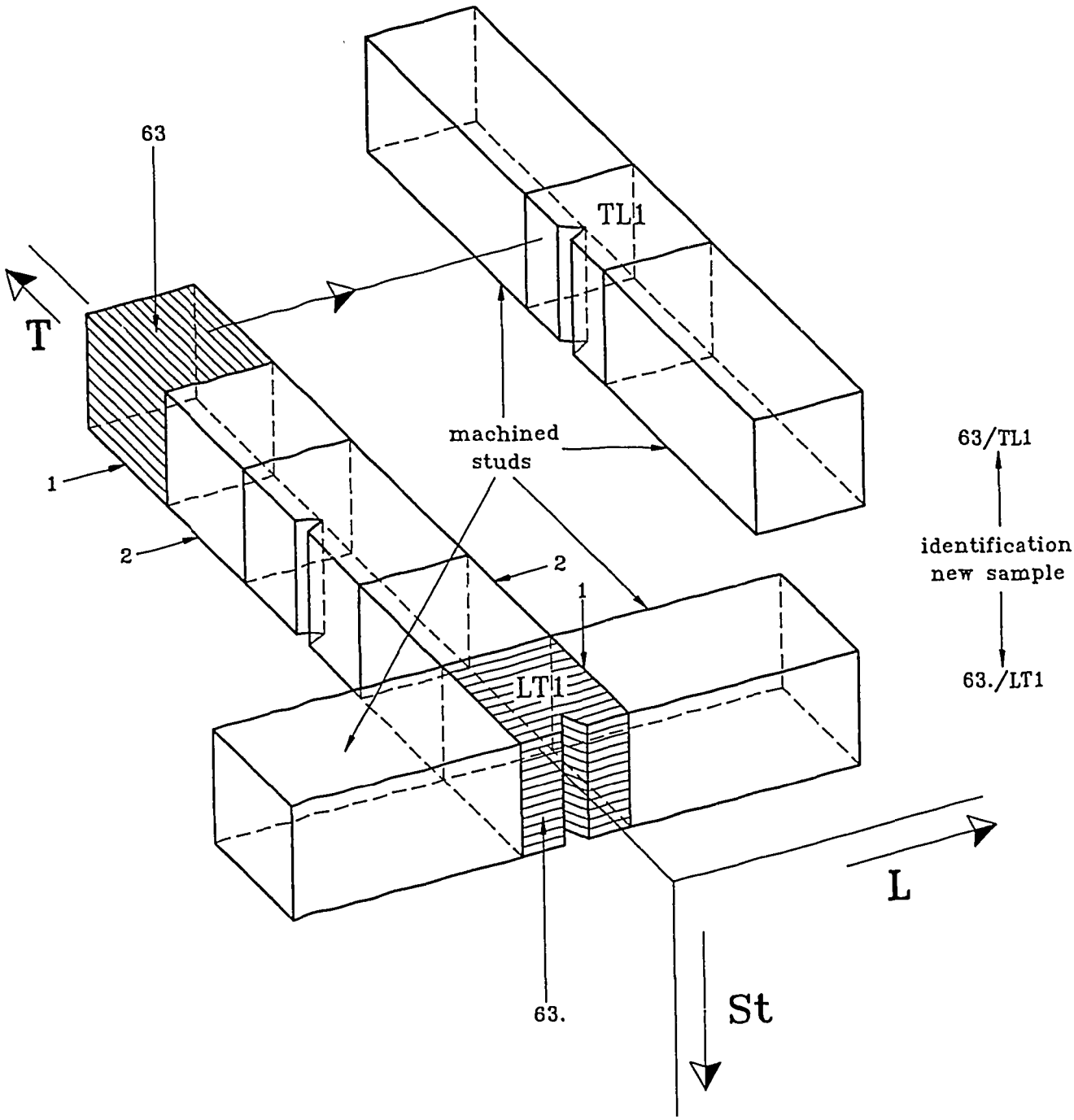

Fig. 5

DEFORMATION CONSTRAINTS BY HARD WELDED ZONES* AND NOTCH ORIENTATION CAUSE SIGNIFICANT ENERGY DIFFERENCES IN Cv- IMPACT TEST

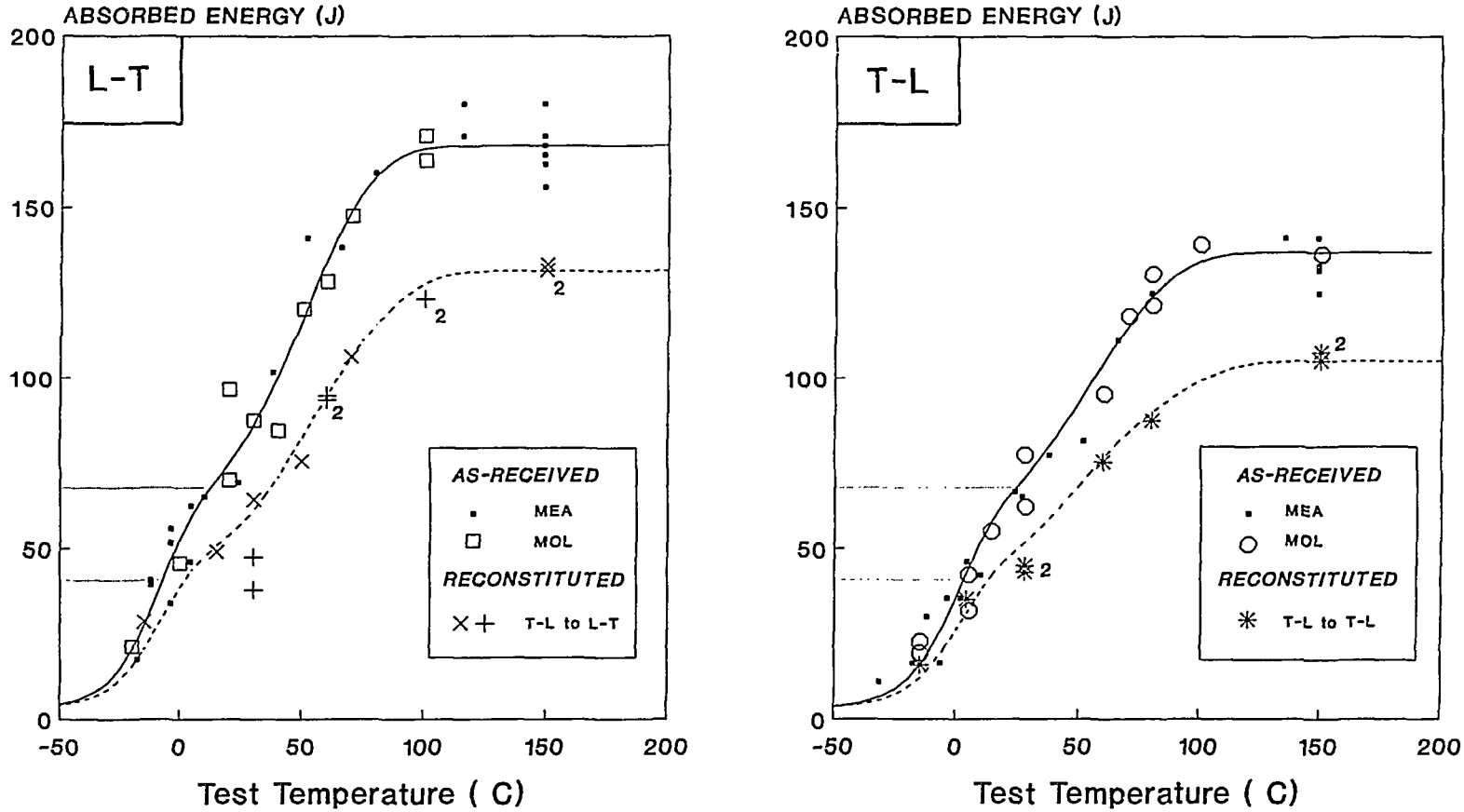

* Cv- Reconstitution: 10x10x10 MM REMNANTS, Plate HSST-03 *Un-irradiated Condition STUD WELDING TESTS PER ASTM E23*

Fig. 6 INVARIANCE OF CV- FRACTURE APPEARANCE TO NOTCH ORIENTATION & RECONSTITUTION

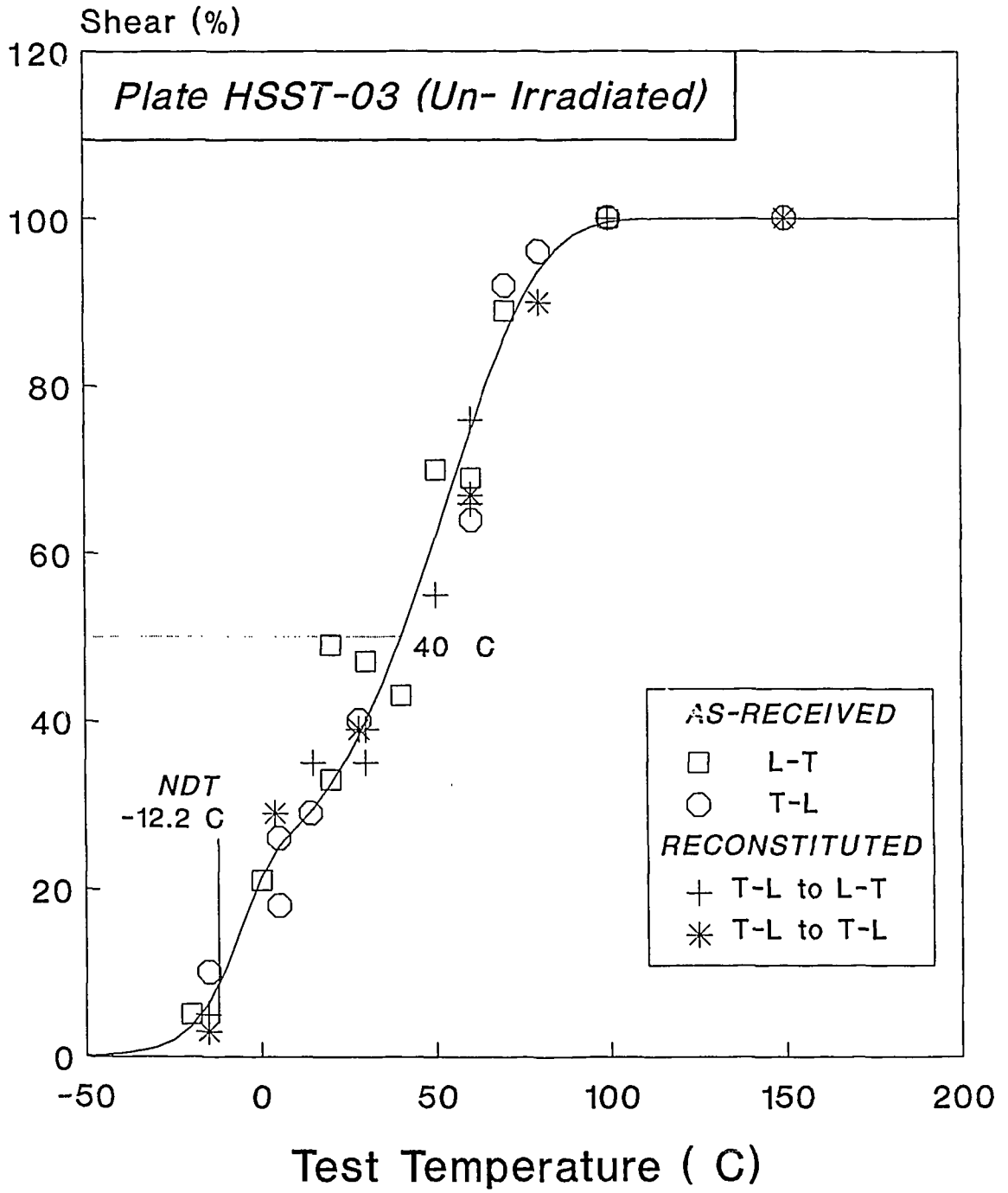

Fig. 7 ENERGY LOSSES FOR ELECTRON-BEAM RECONSTITUTION OF 10x10x10 MM. UNIRRADIATED 22NiMoCr37 Cv-REMNANTS

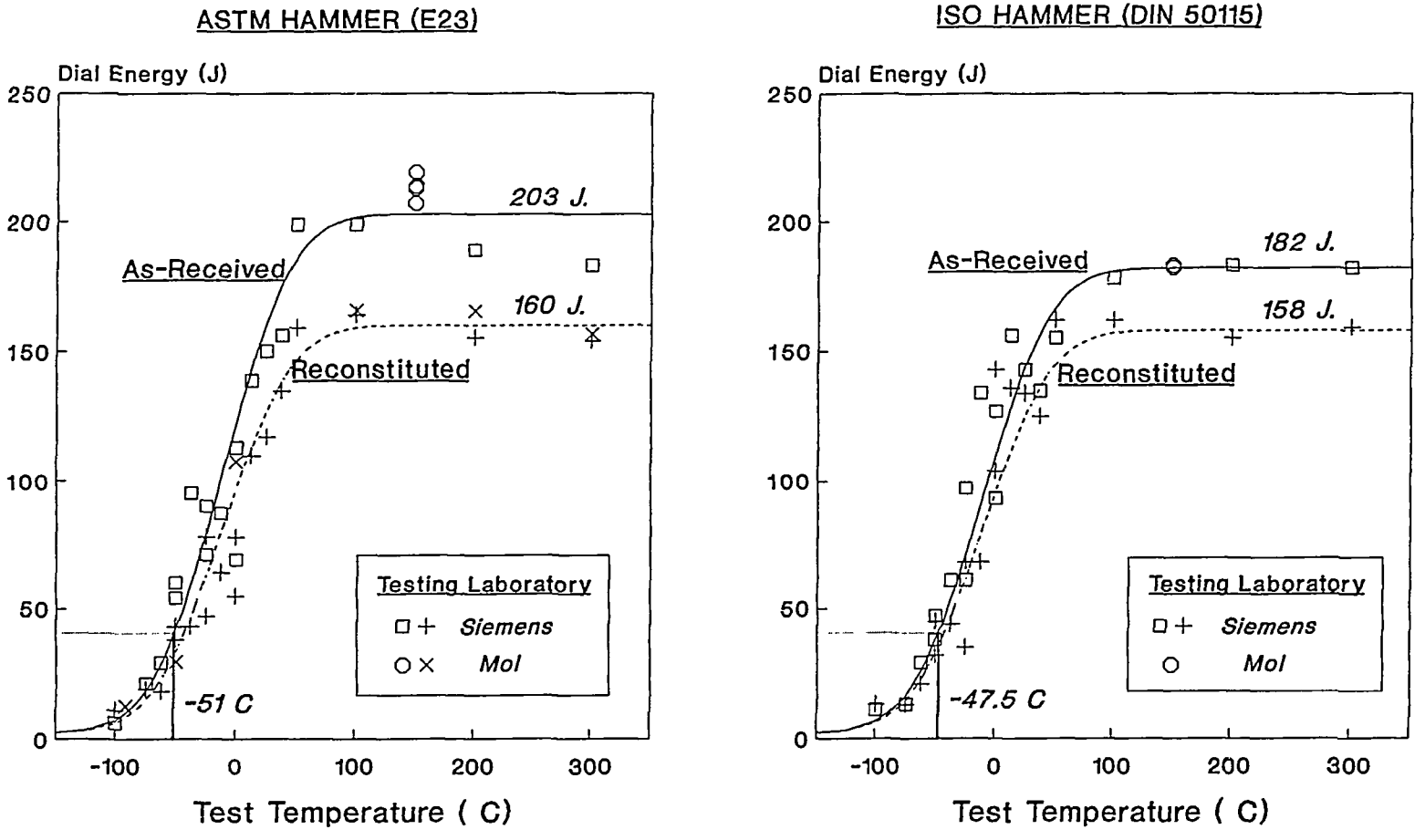

BASE METAL, S-L NOTCH ORIENTATION

FITS CONSTRAINED TO EMPIRICAL REPRESENTATION BY *TANH* FUNCTIONS

Fig. 8 FRACTURE APPEARANCE: 22NiMoCr37 BASE TESTED BEFORE AND AFTER EB RECONSTITUTION

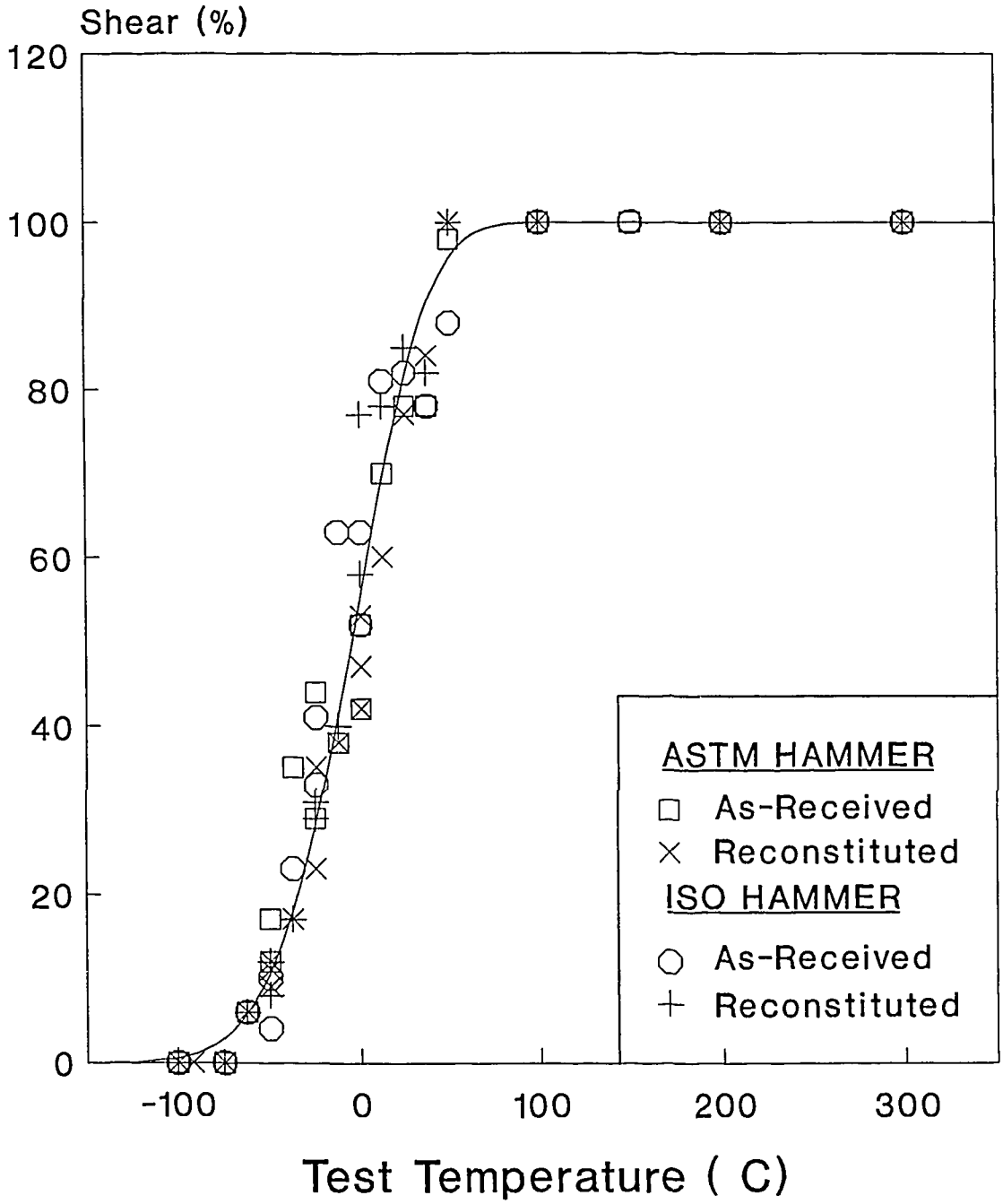

Fig. 9 CORRECTION SCHEME FOR NOTCH RE-ORIENTATION

(BY RECONSTITUTION OF 10x10x10 MM CHARPY-V REMNANTS)

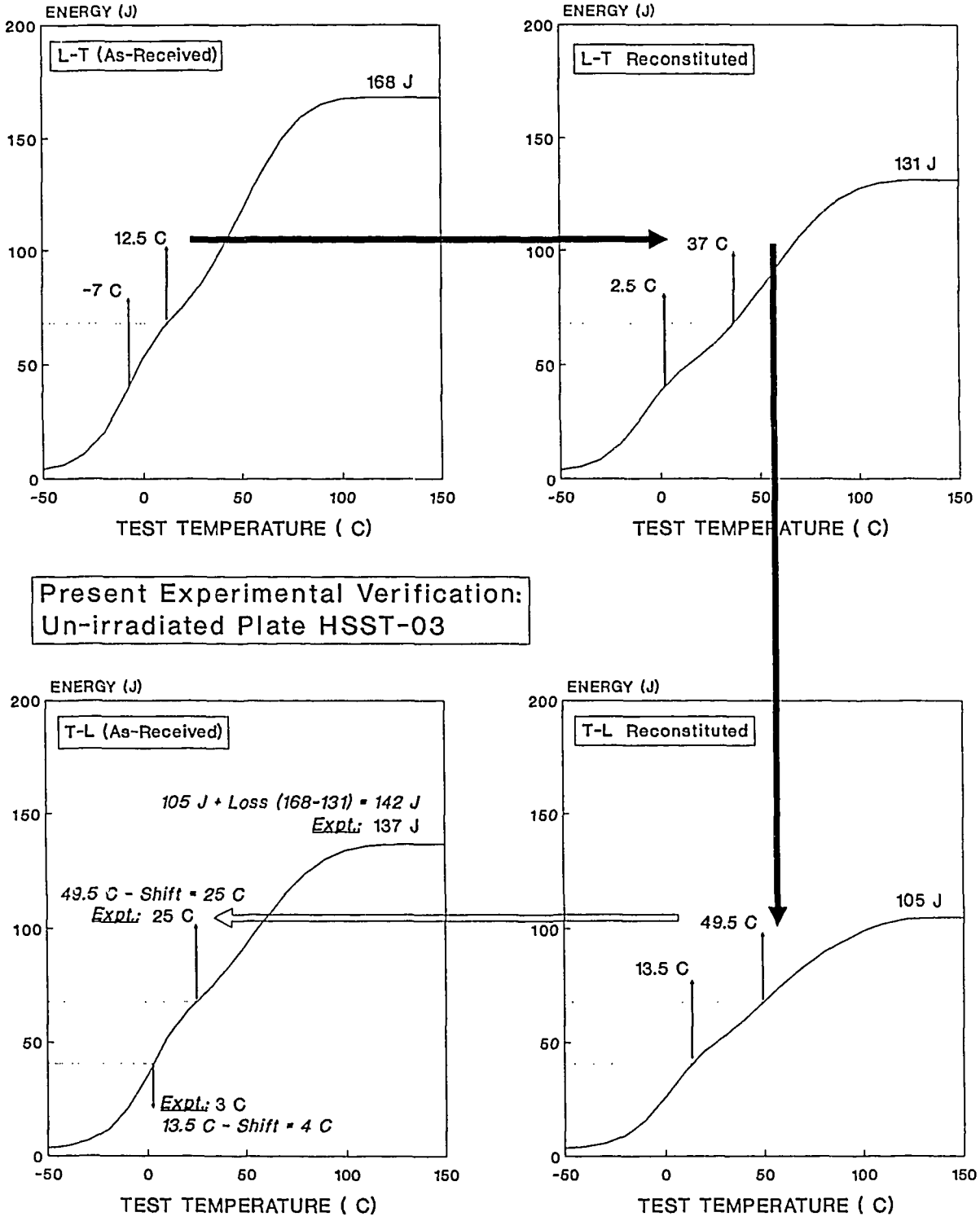

Fig. 10 Cv-RECONSTITUTION: Energy Losses for 10x10x10 mm Remnants

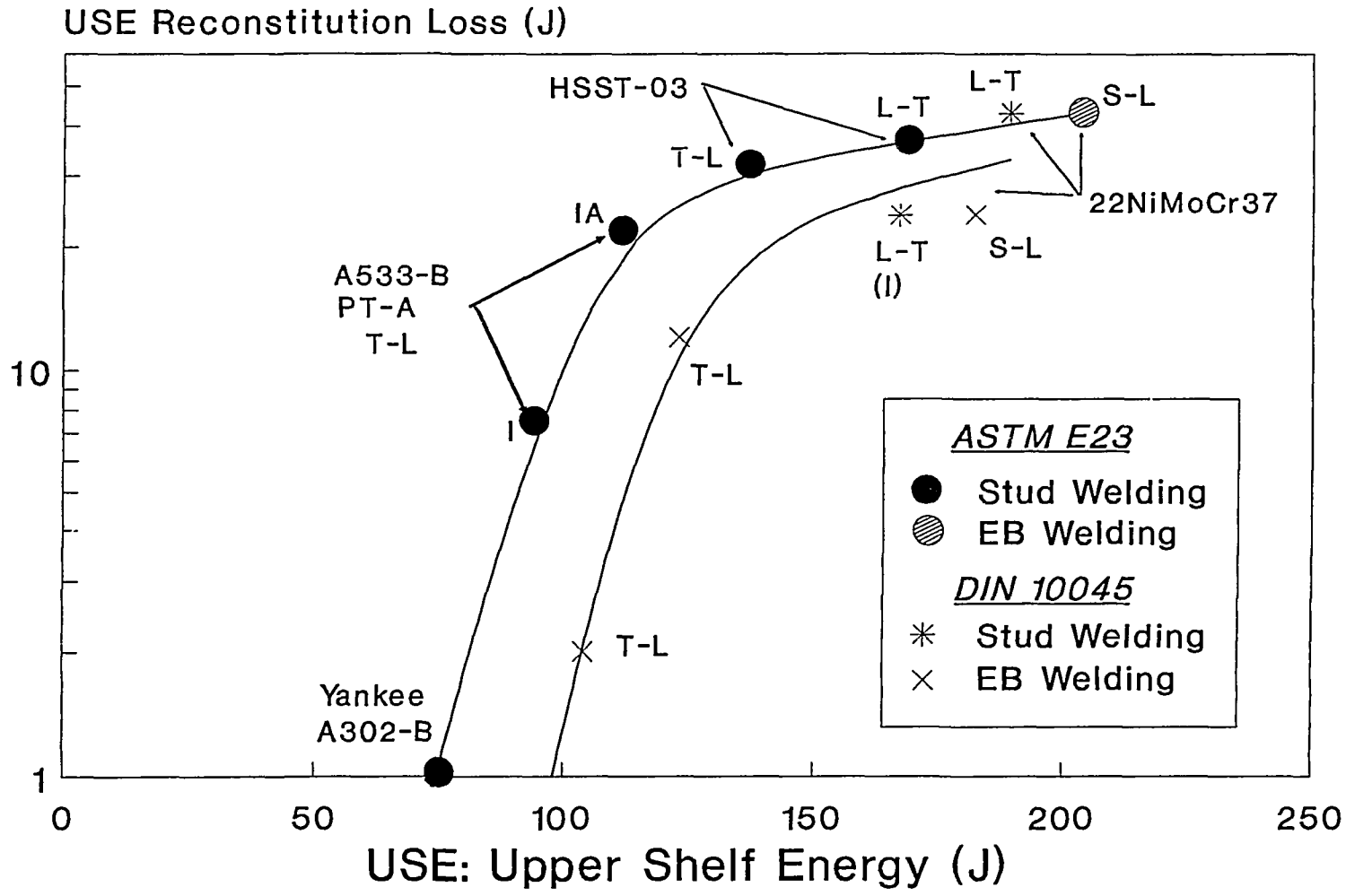

Fig. 11 EVALUATION OF MINIATURE Cv- TEST RESULTS

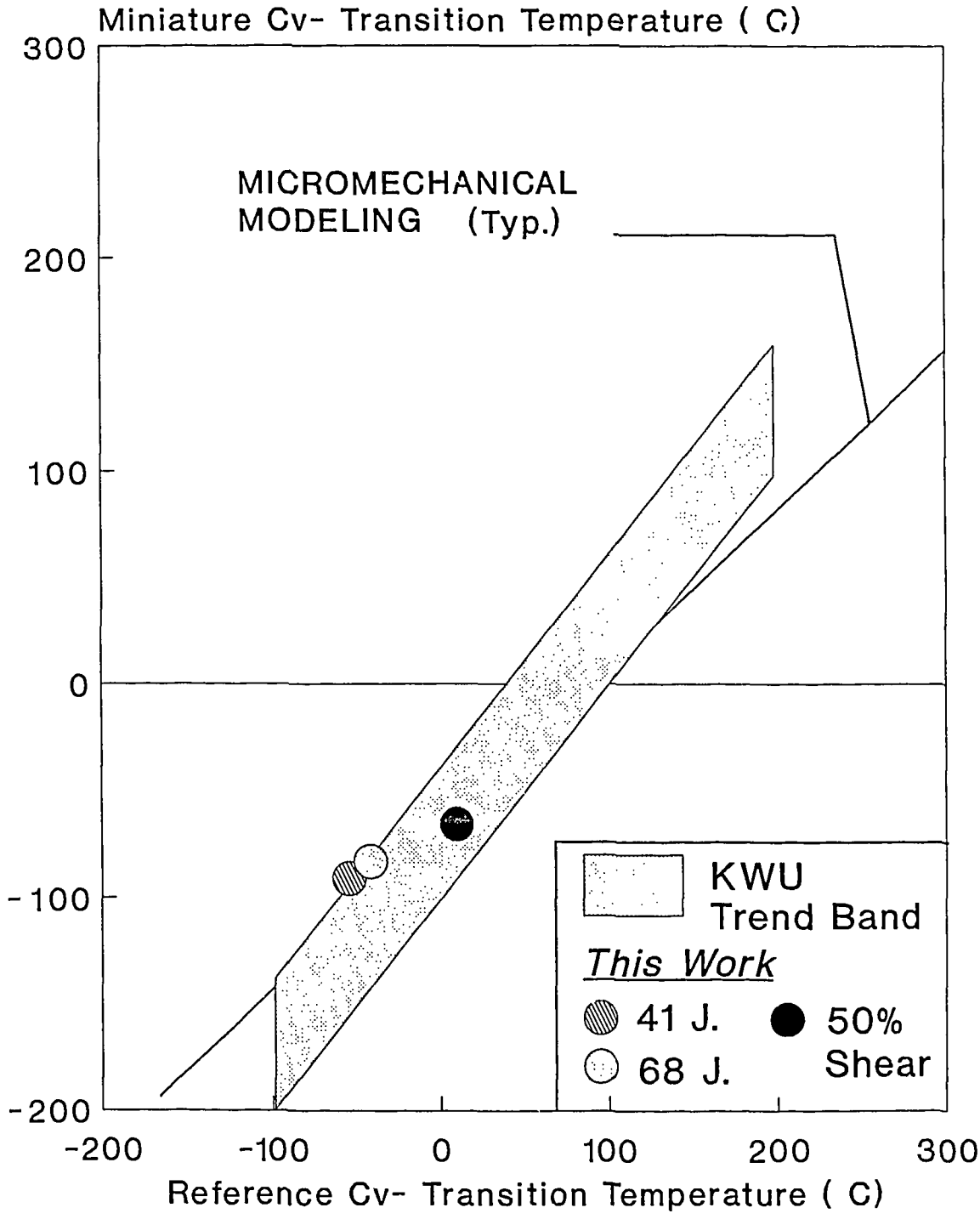

Fig. 12 INITIAL CALIBRATION OF MINIATURIZED CHARPY-V IMPACT TEST

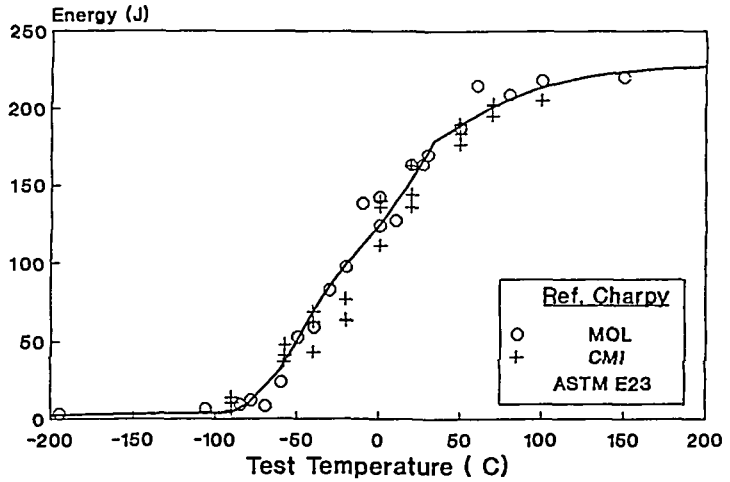

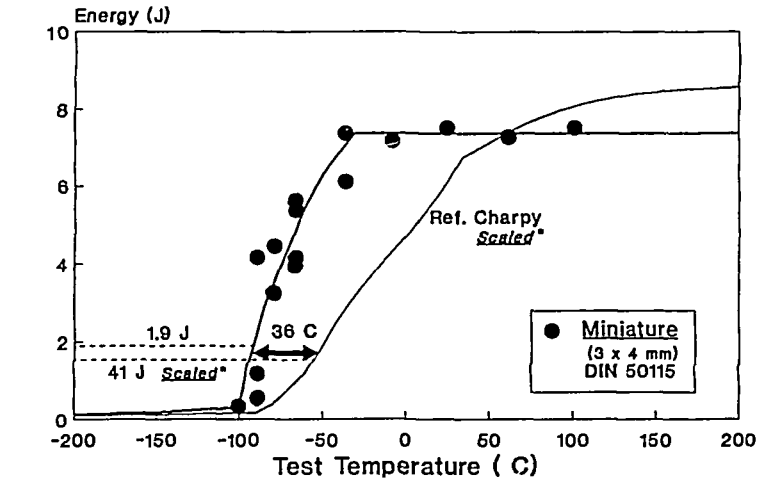

* Volume Scaling (x 1/ 26.5)

Doel 4 Base Metal
Un- Irradiated

Lateral Expansion

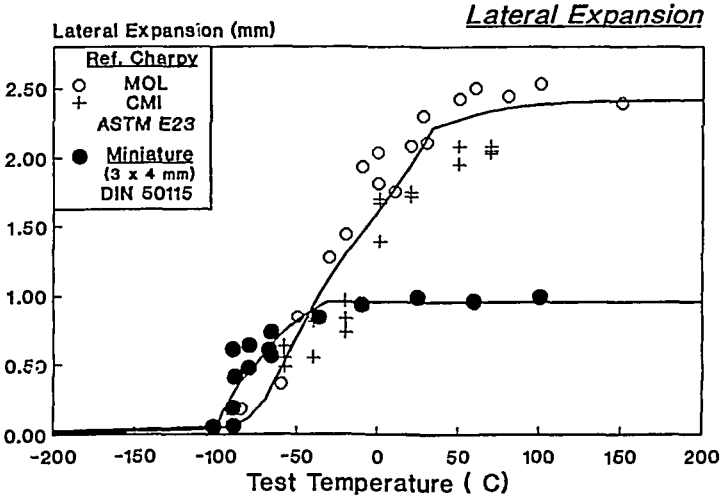

Fracture Appearance

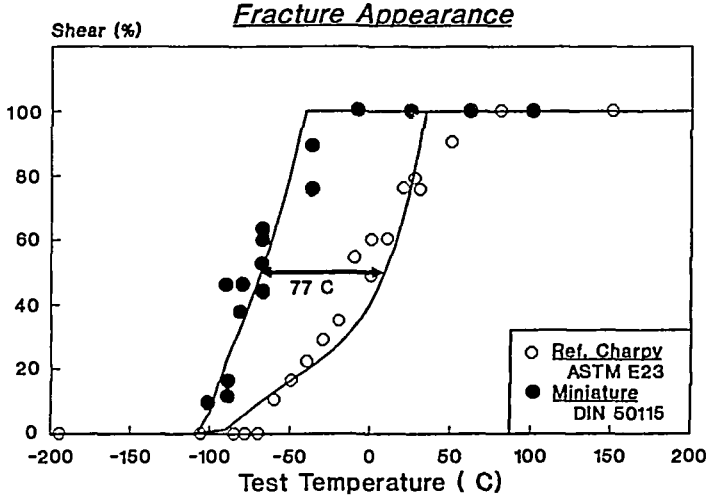

Fig. 13

GUIDELINES TO DAMAGE MODELING OF RPV STEELS

DUCTILE- BRITTLE TRANSITION TEMPERATURE *(DBTT)*

- *GENERAL YIELD STRESS*
  = CLEAVAGE FRACTURE STRESS
- For Temperature > DBTT:
  Strain Hardening Needed for Fracture
  (Plastic Deformation)

"CLASSICAL" MATRIX HARDENING

- Irradiation Creates Obstacles
  to Movement of Dislocations
  (for ex., Precipitates)
- Material Flow Is Hampered
  i.e. Yield Stress Increases
- *DBTT INCREASE PROPORTIONAL TO YIELD STRESS INCREASE*

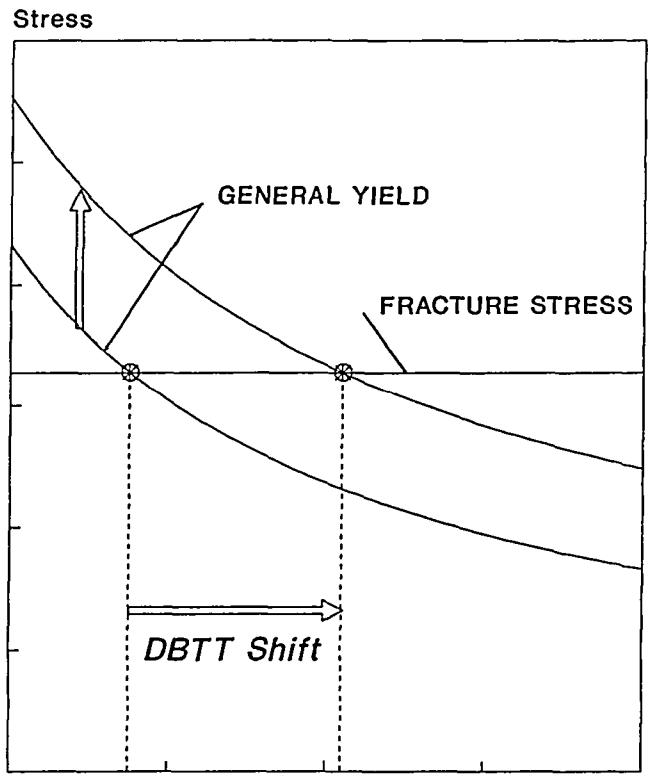

Fig. 14 USE OF INSTRUMENTED CHARPY-V LOAD-TIME TRACES

Typical Signal
(Transition Temperature Range)

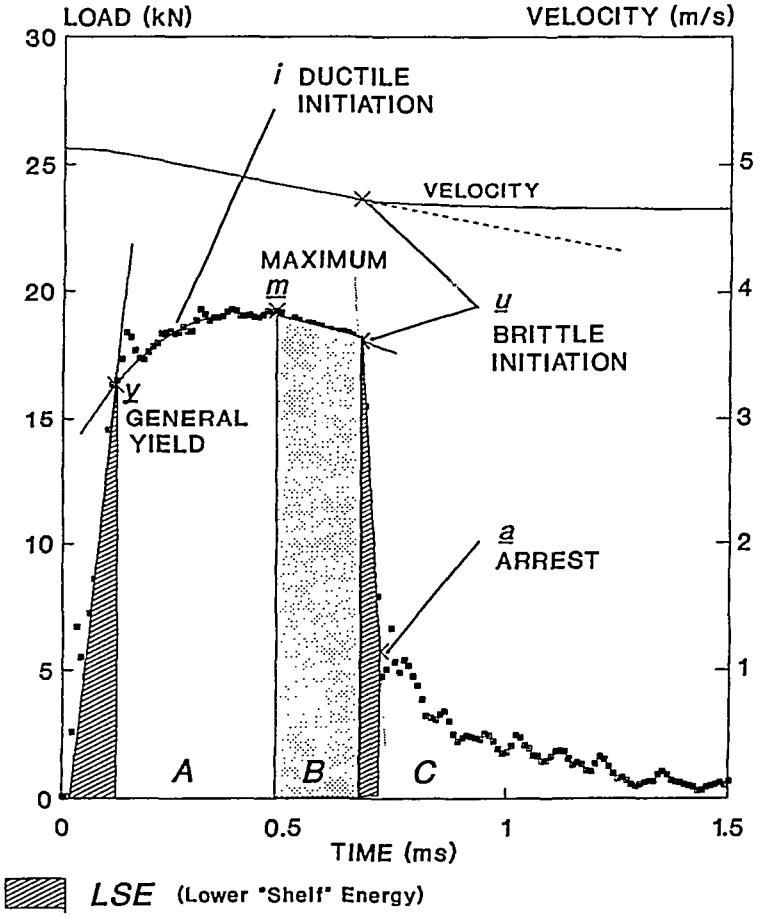

Typical Load Diagram and Energy Partitioning

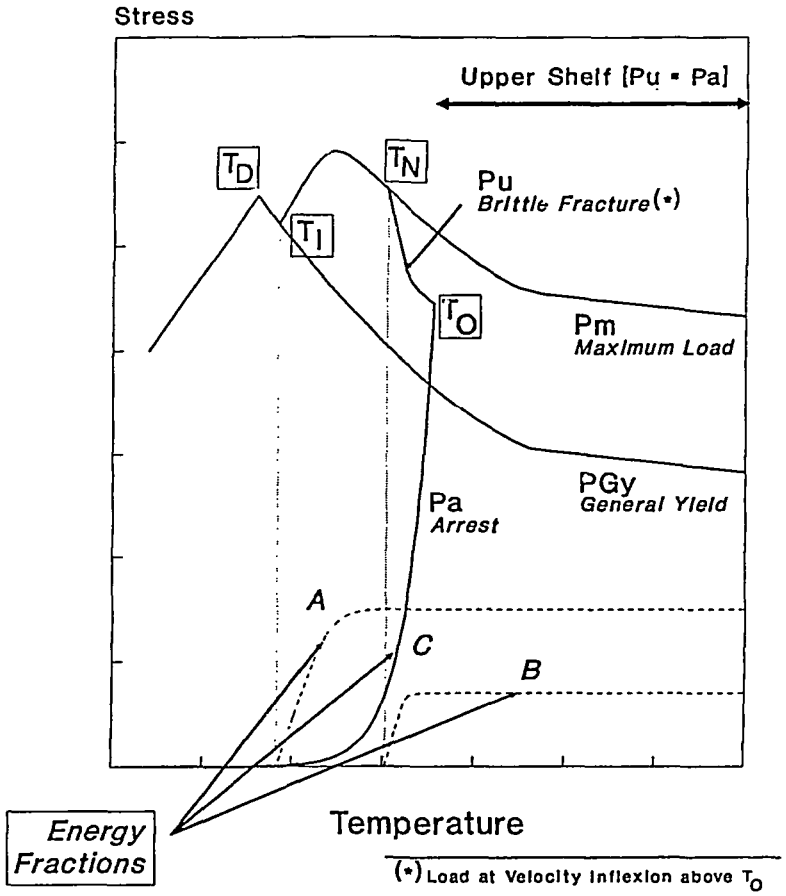

Fig. 15 Inadequacy of 41 J. Charpy-V Indexation

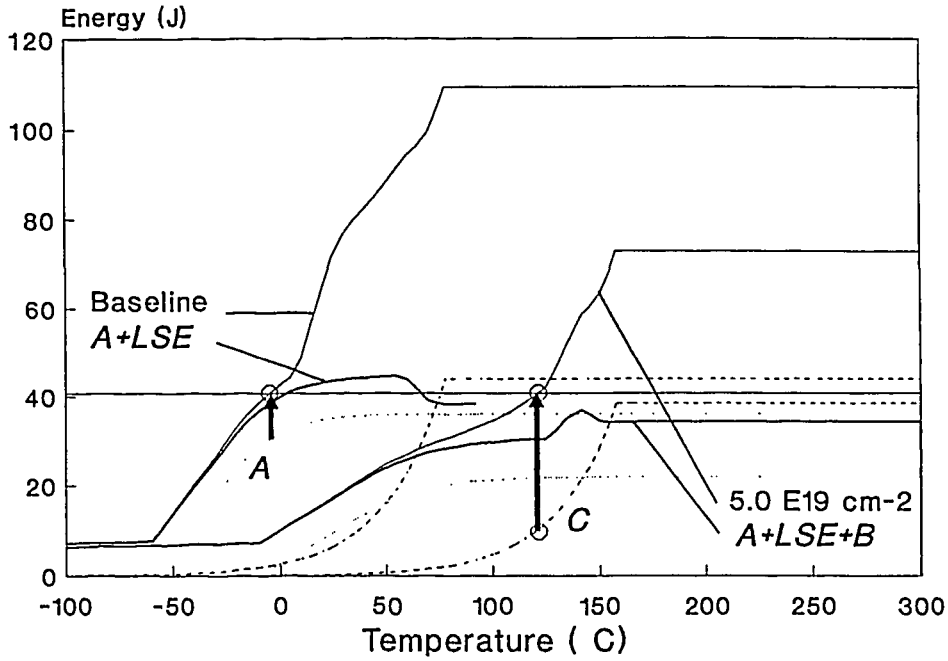

Upon Irradiation of Considered Steel

CONTROL OF 41 J. TEMPERATURE "SHIFTS"

FROM PRE-MAXIMUM ENERGY FRACTION IN BASELINE TO POST-ARREST ENERGY FRACTION AT 5 E19 cm-2

BIASING 41J TOUGHNESS FIX

Fig. 16 **Correlation of Fracture Appearance to Instrumented Cv- Impact Load Diagram**

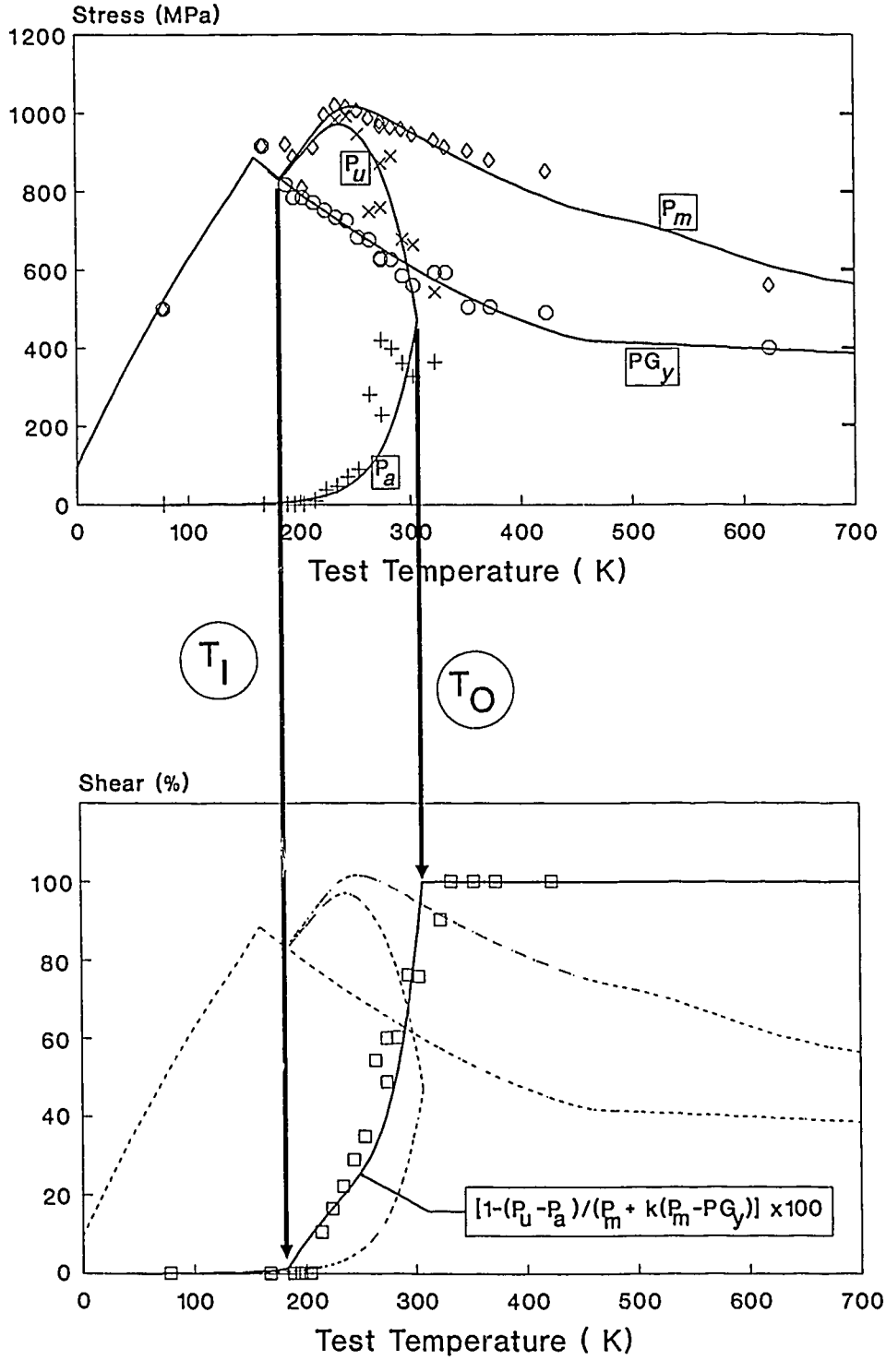

Doel-4 Un-Irradiated Base Metal

Fig. 17 Influence of Irradiation: Cv- Load Diagrams and Shear

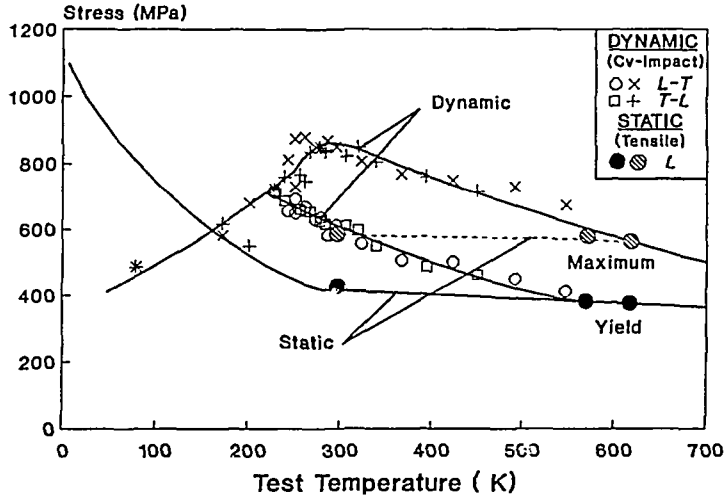

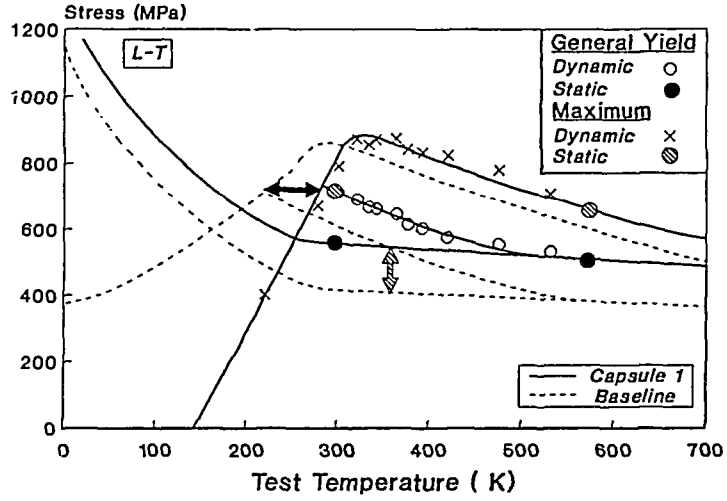

Baseline

1.8 E19 cm-2 (>1 MeV)

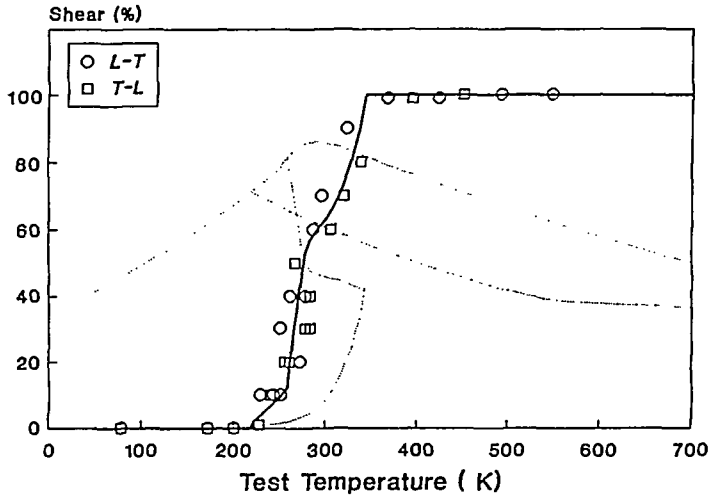

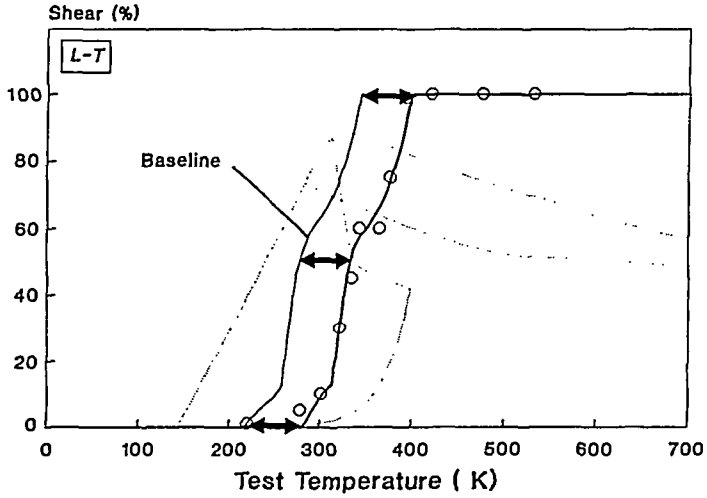

Fig. 18 INVARIANCE OF Cv- LOAD DIAGRAM AND FRACTURE APPEARANCE

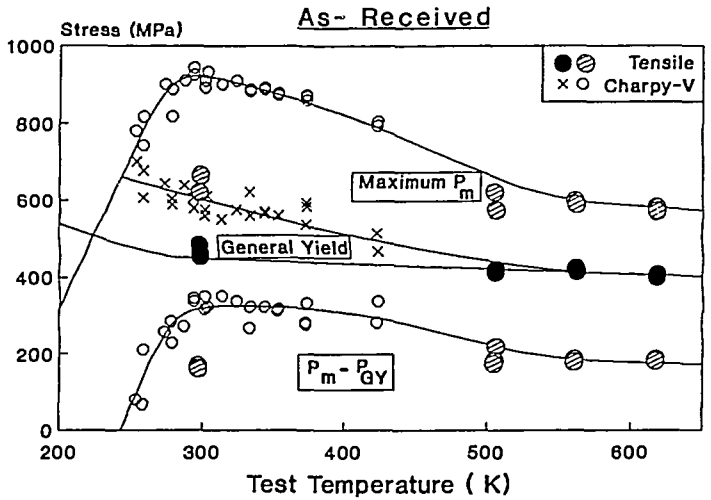

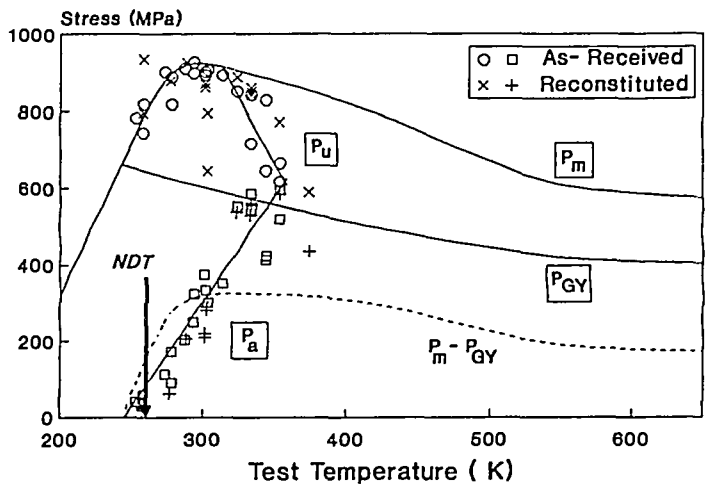

A533-B Plate HSST-03 (Un-Irradiated) Cv- Tests with ASTM Hammer
L-T & T-L Reconstituted Data: 10 x 10 x 10 mm Remnants

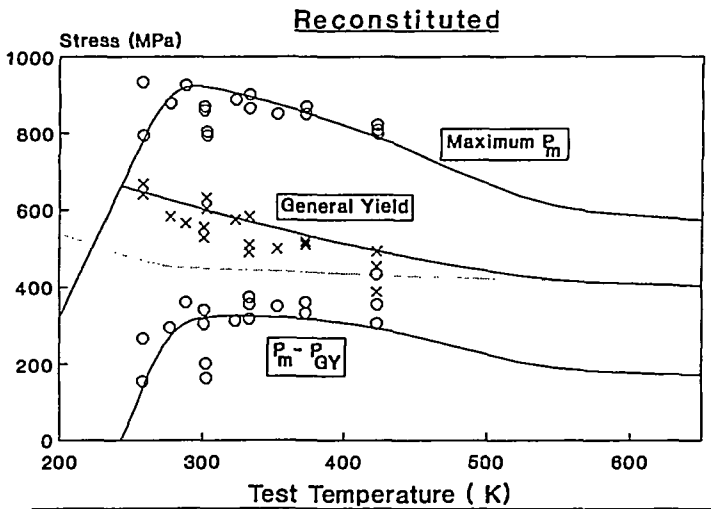

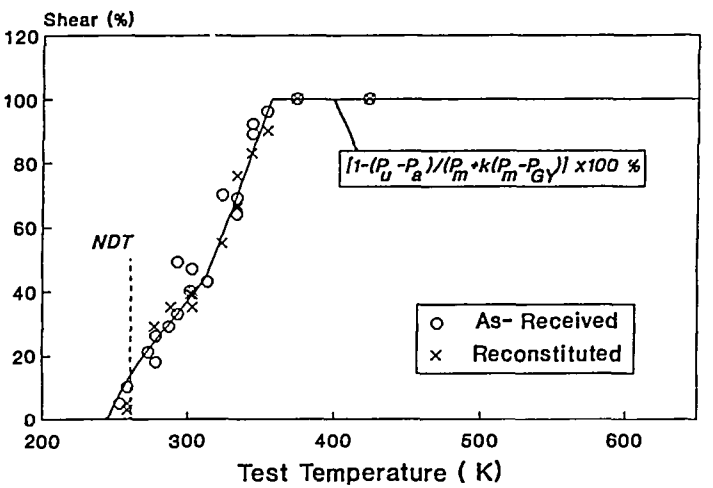

All Data Fitted by Unique Set of Parameters

Fig. 19 Quality Assurance for Cv- Impact Load Diagram Procedure

Siemens Research Plate (Reiff et. al. 1991)

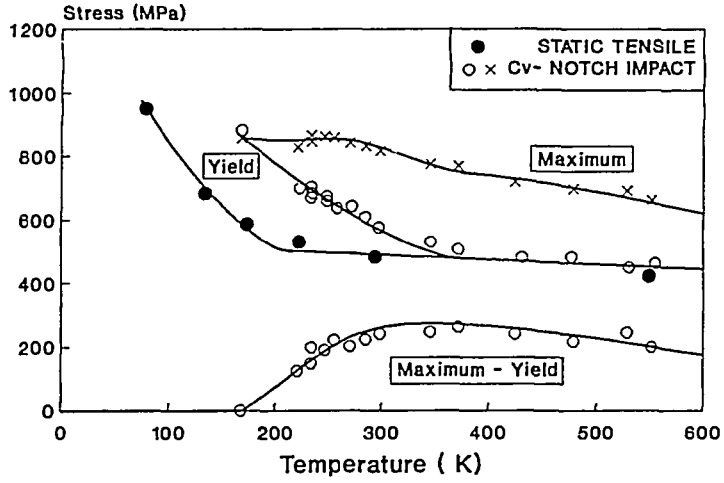

Forging Ring for EGF Round Robin on 'Local Approach'

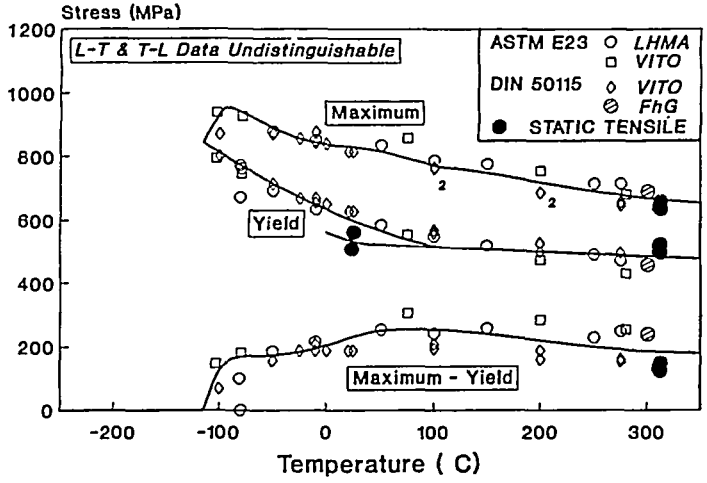

22NiMoCr37 Unirradiated

Reconstitution of KKW-1 Surveillance Plate

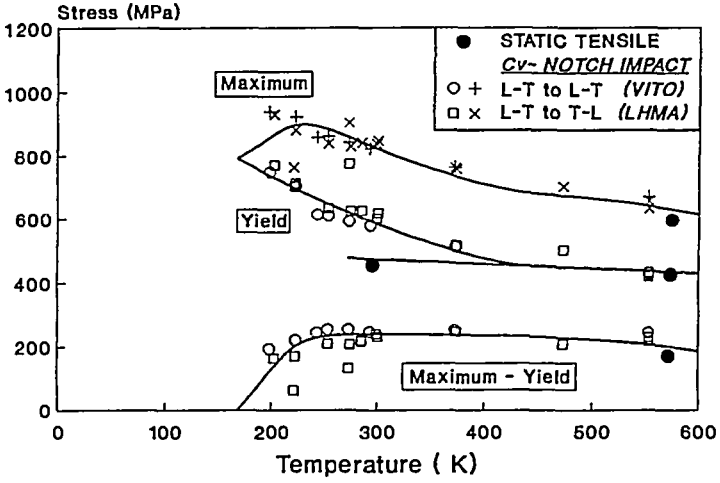

- For Three Considered Steels:
  Uniaxial Static Yield and Cv- Impact General Yield: Consistent
- Diagram Independent of
  - Notch Orientation
  - Hammer Geometry
  - Reconstitution
- Diagram Data Scatter: Usually Small
- Good Interlaboratory Agreement of Tests at LHMA, VITO SIEMENS, FhG

Fig. 20 mean strain - mean stress
experimental versus calculus

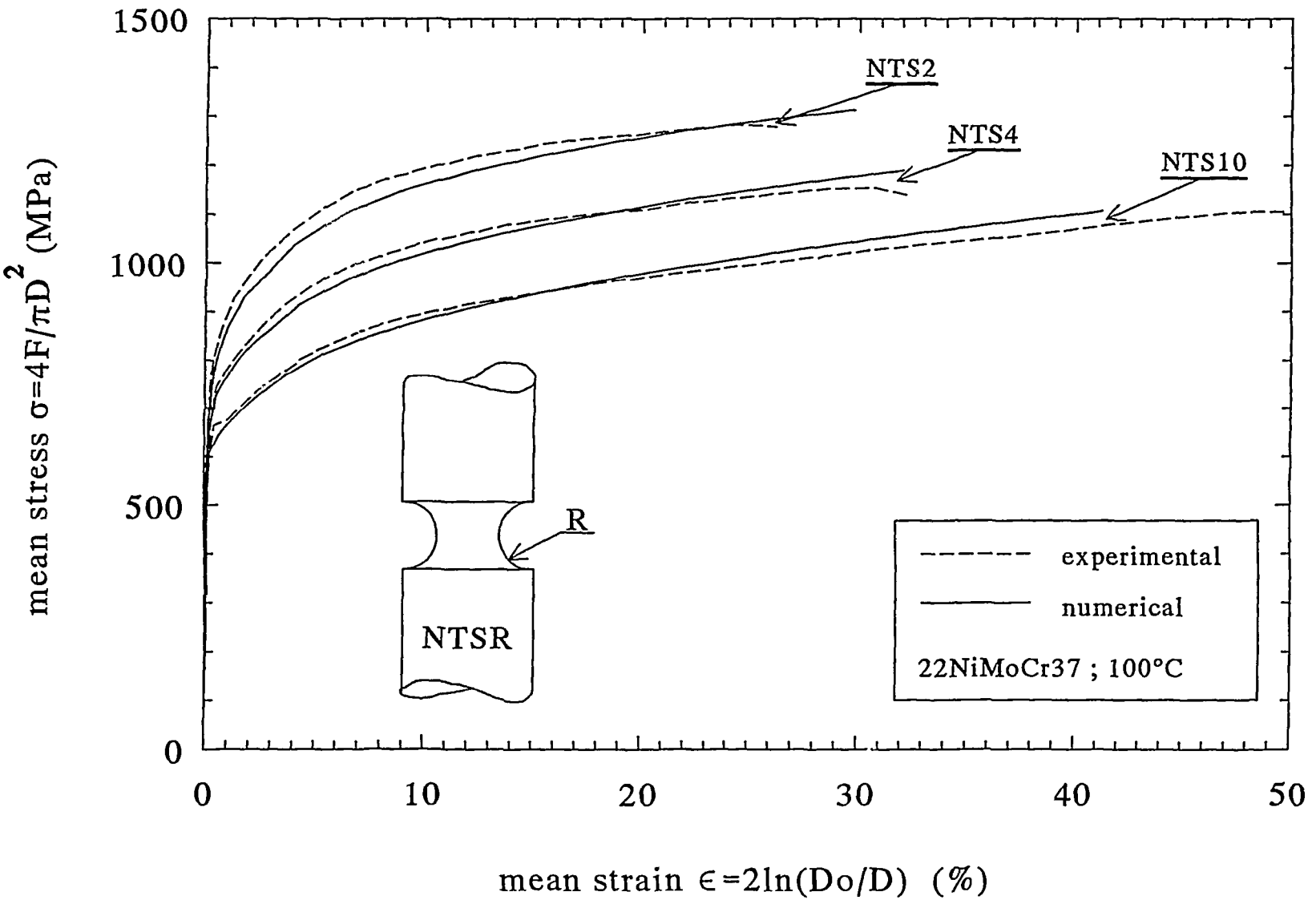

Fig. 21 damage evolution with mean strain

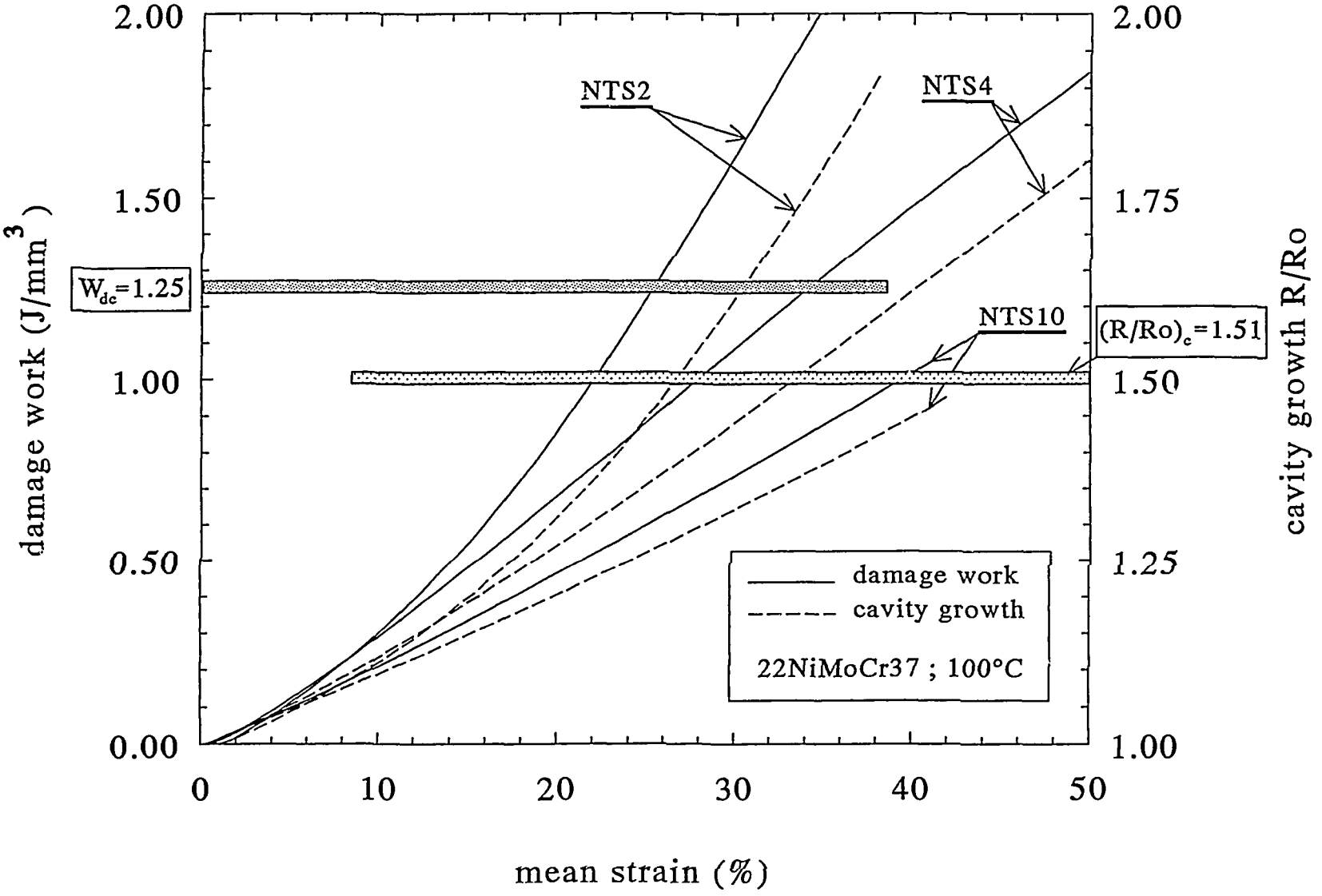

Fig. 22

TENSILE TEST DATA FOR DOEL-I,-II WELDS

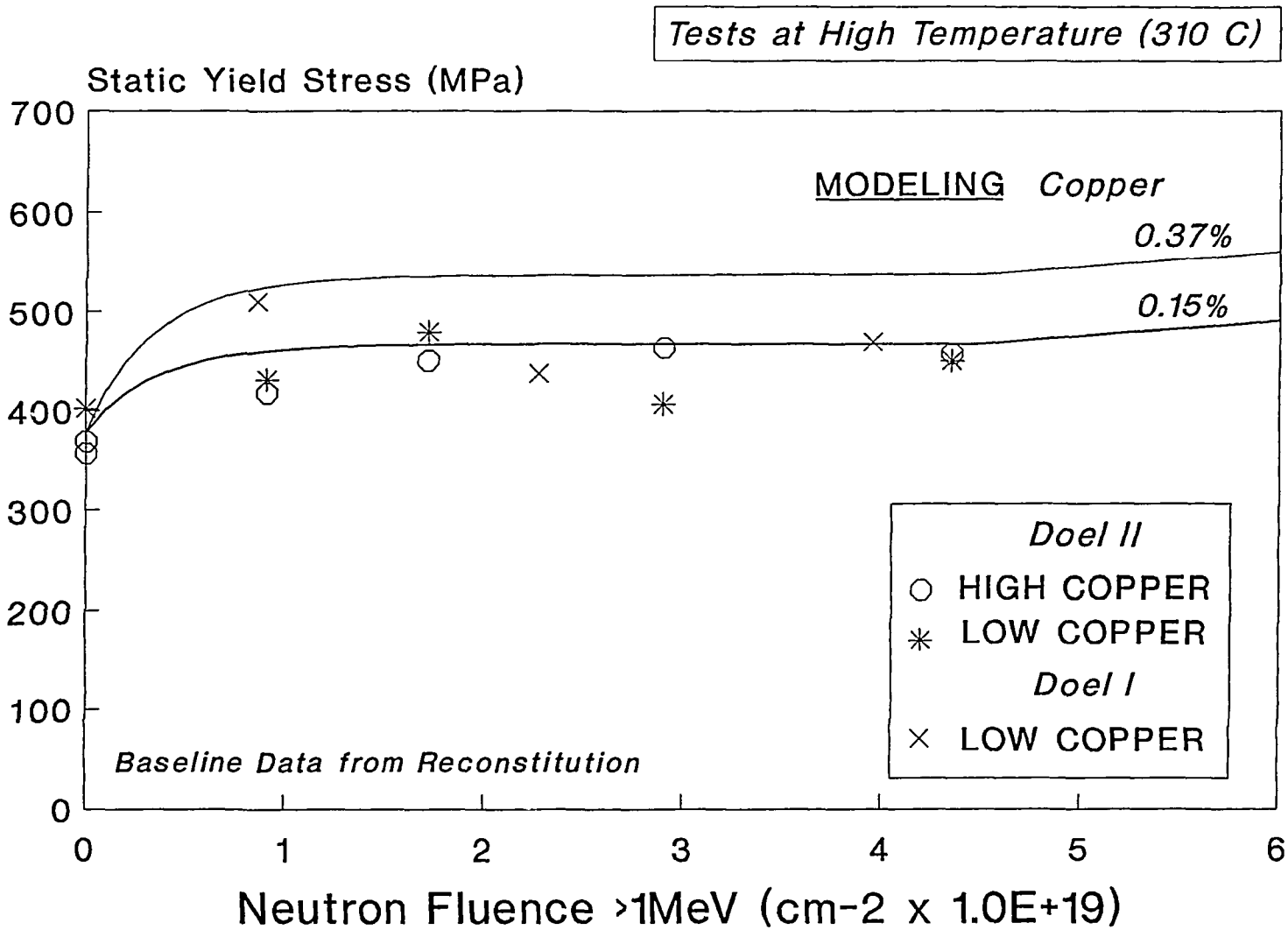

Fig. 23

A302B PLATE TENSILE YIELD STRENGTH AFFECTED BY *3 DISTINCT DAMAGE MECHANISMS*

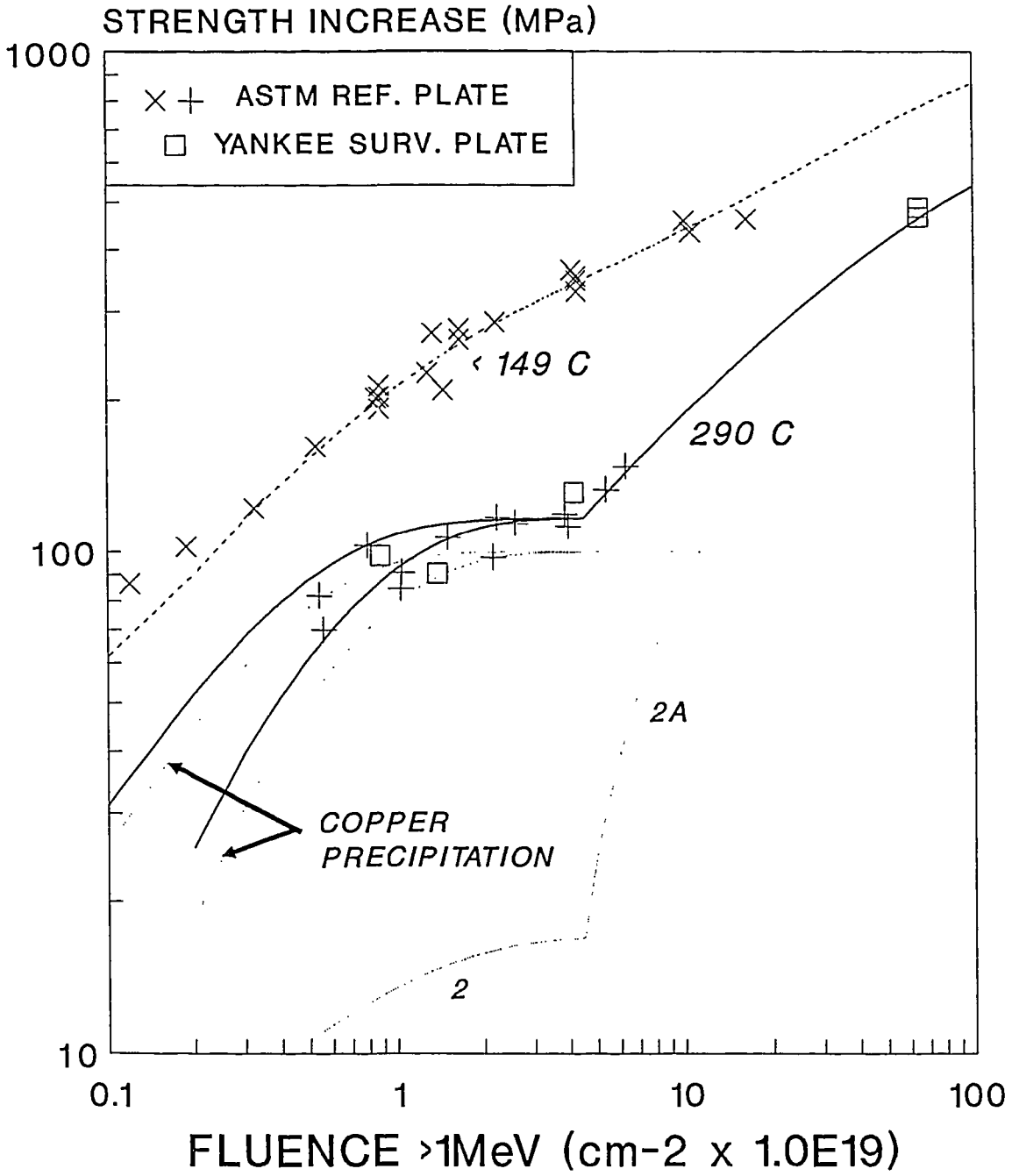

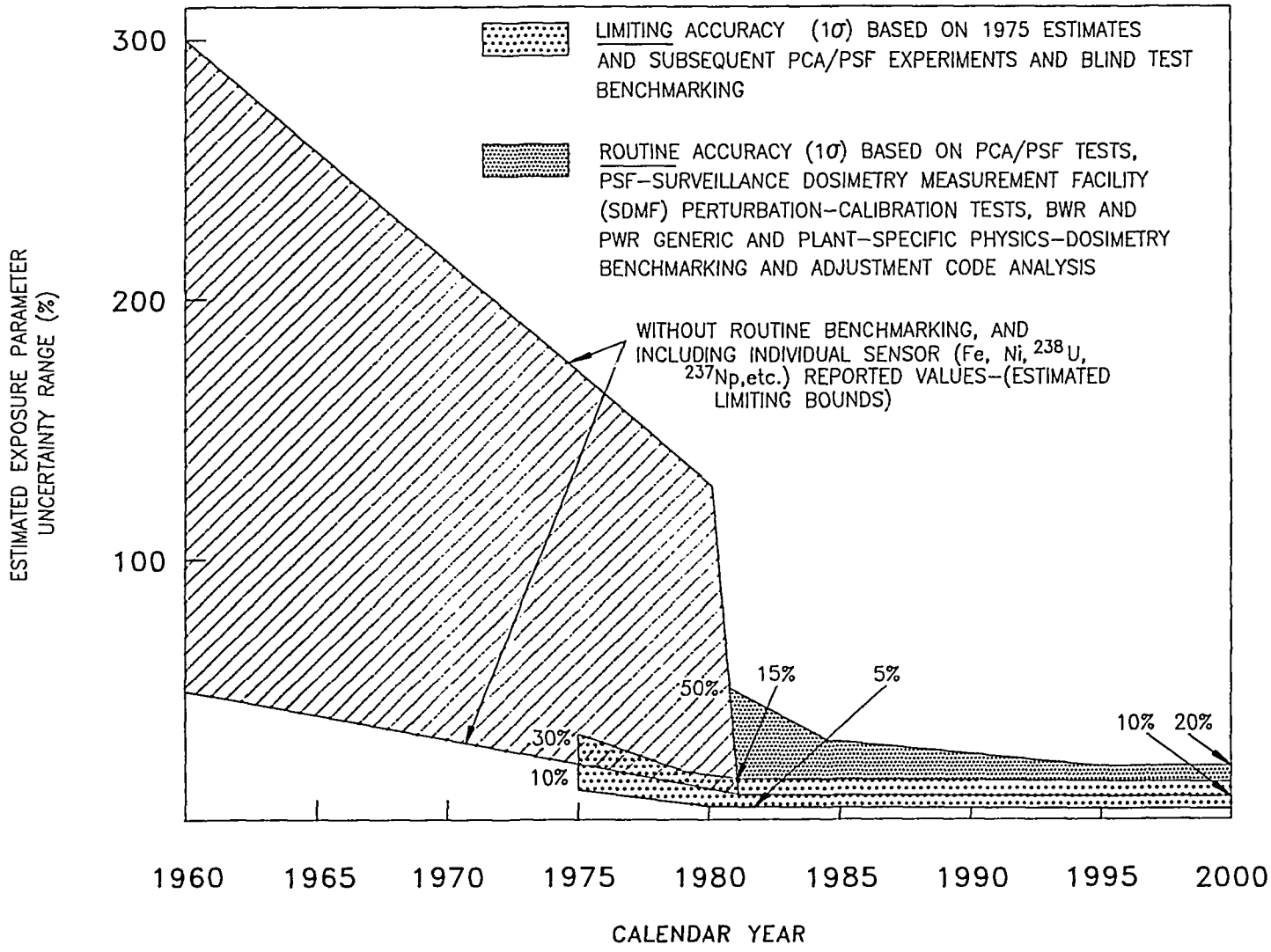

Fig. 24: Estimated exposure parameter uncertainties obtained from FSAR, surveillance capsule reports, and recent efforts of the LWR–PV–SDIP program.